Hudson Laboratories
of
Columbia University
Dobbs Ferry, New York

TECHNICAL REPORT No. 80

The Spark Gap as an Acoustic Source

by
M. Vertner Brown
and
James Ricard

Contract Nonr - 266 (84)

CU-101-62-ONR-266-Phys.

Hudson Laboratories
of
Columbia University
Dobbs Ferry, New York

Robert A. Frosch
Director

Technical Report No. 80

THE SPARK GAP AS AN ACOUSTIC SOURCE

by

M. Vertner Brown

and

James Ricard

October 30, 1959

UNCLASSIFIED

This report consists
of 42 pages

Copy No. 88
of 100 copies

This work was supported by the Office of Naval Research under Contract Nonr-266(84). Reproduction in whole or in part is permitted for any purpose of the United States government.

ABSTRACT

This report describes and evaluates a model system for studying the transmission of acoustic signals through the water. Spark sources were studied with special reference to whether the acoustic signals generated by sparks scale with those generated by explosions. It is shown that they do not.

The surface reflection of these pulses was also studied. A phase shift as a function of frequency and a change in pulse shape as a function of angle of incidence were observed.

An extended series of experiments was performed, each experiment incorporating new parameter controls and/or improved apparatus and techniques, the most successful of which are reported here. Particular attention was directed to the problem of reducing stray arrivals through proper support of the hydrophones and the spark gap.

CONTENTS

I. DESIGN AND CALIBRATION

Tank Facilities for Acoustic Studies

A steel tank, 54 in. by 60 in. by 49 in., was fitted with an acoustic bench on which the spark gap and the hydrophones could be positioned accurately. The accessory equipment included:

(1) A power supply adequate to charge a 2-μf capacitor to 2000 v with a repetition rate not exceeding 5/sec. The power supply was adjustable to deliver any voltage between 0 and 2600 v. The capacitor was discharged through an underwater spark gap by pulsing a 4C35 thyratron (see Fig. 1).

(2) A crystal-controlled oscillator providing 100-kc and 1000-kc timing pips.

(3) Passive probes for matching the hydrophone probes to coaxial cable. The gain was 0.7 , 3 db down at 2.4 mc and 50 cps (see Fig. 2).

(4) Cathode followers for matching hydrophones to coaxial cable. The gain was 0.7 , 3 db down at 2 mc and 180 cps (see Fig. 3).

(5) 20-db amplifiers for matching hydrophones to coaxial cable (3 db down at 5 mc and 800 cps)(see Fig. 4).

(6) A variety of $BaTiO_3$ hydrophones using crystals ranging from 1/16 to 1/4 in. in diameter.

(7) A 535 Tektronix scope and a 531 Tektronix scope.

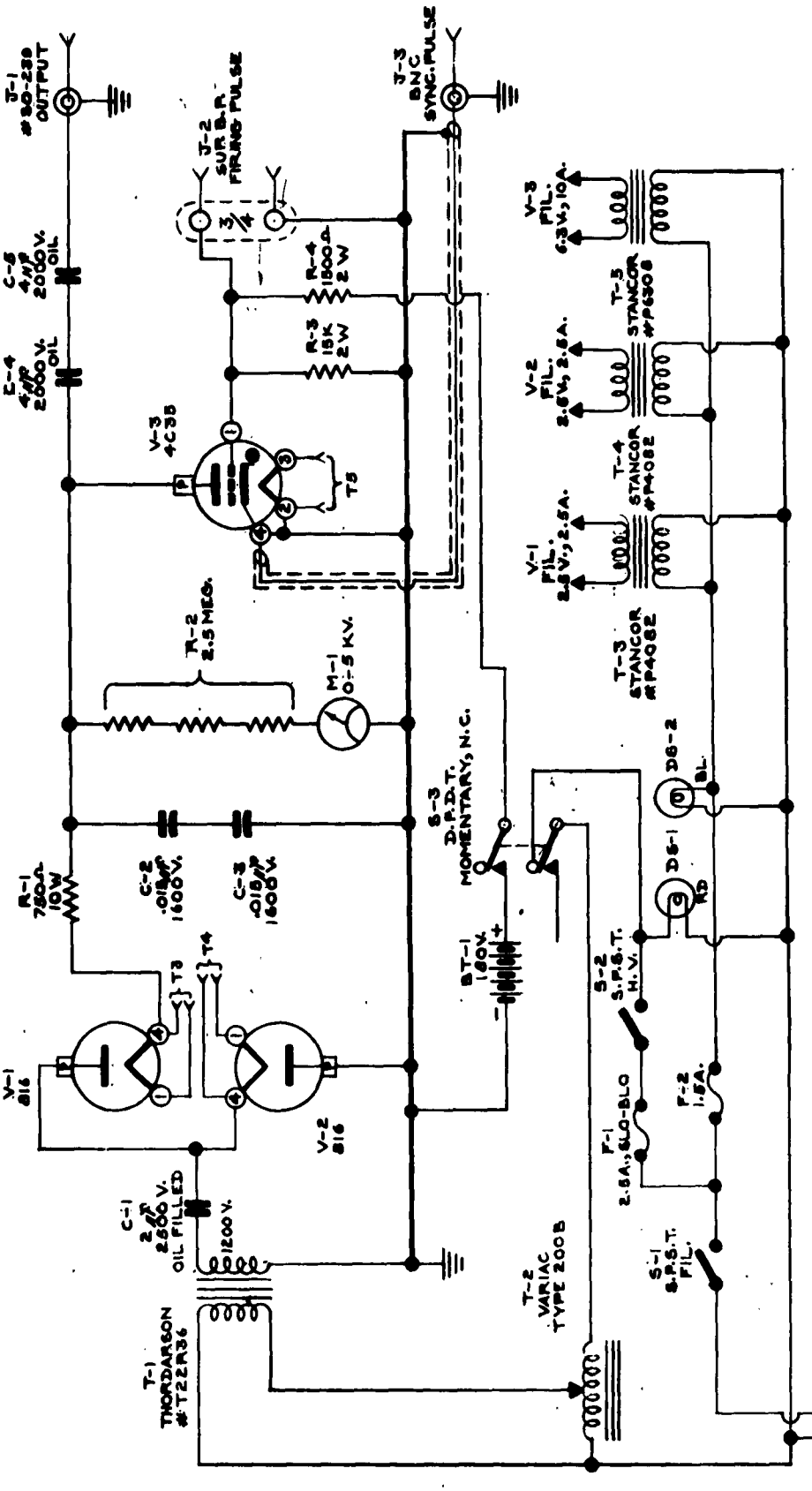

Fig. 1 High voltage supply and spark control

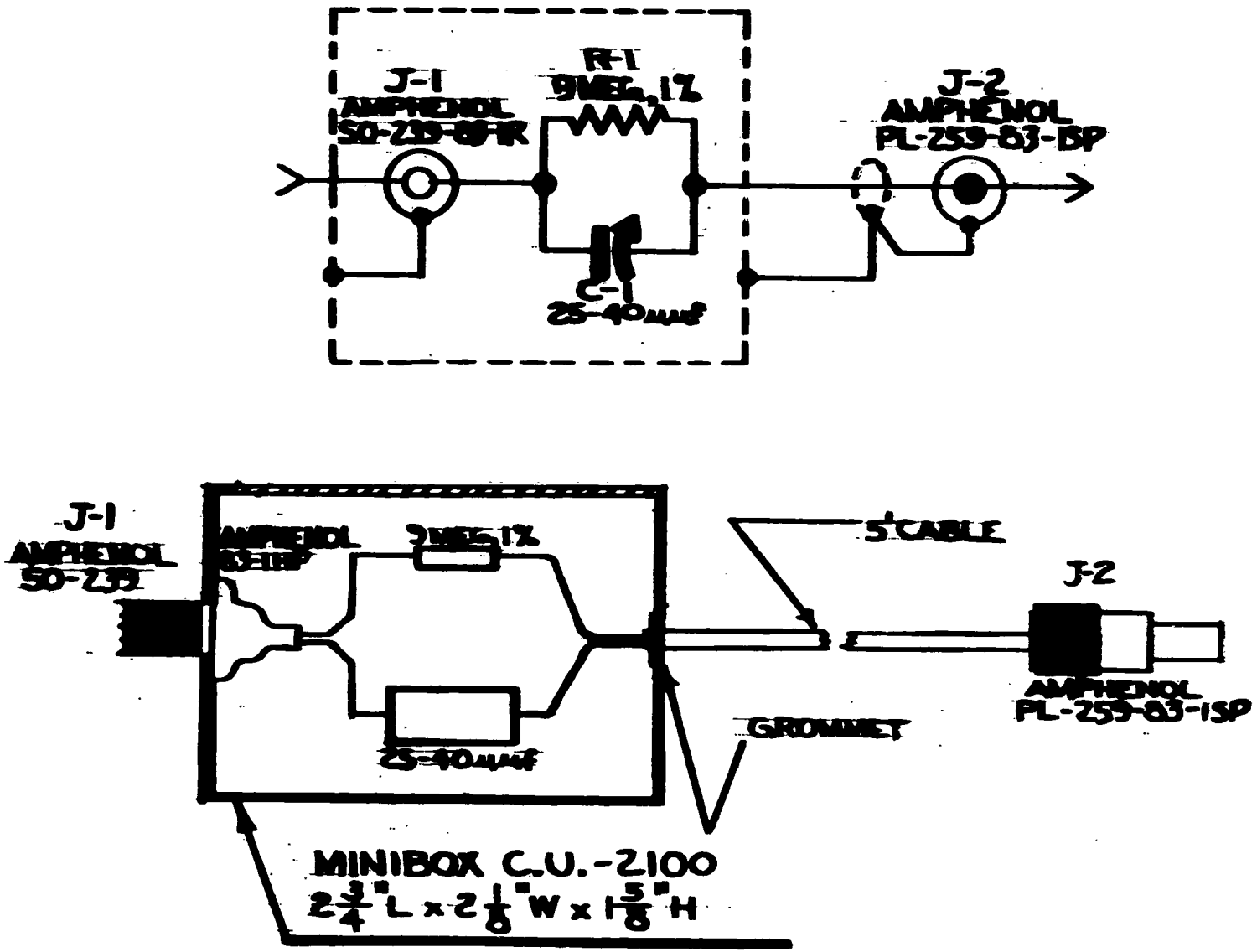

Fig. 2 Compensated probe

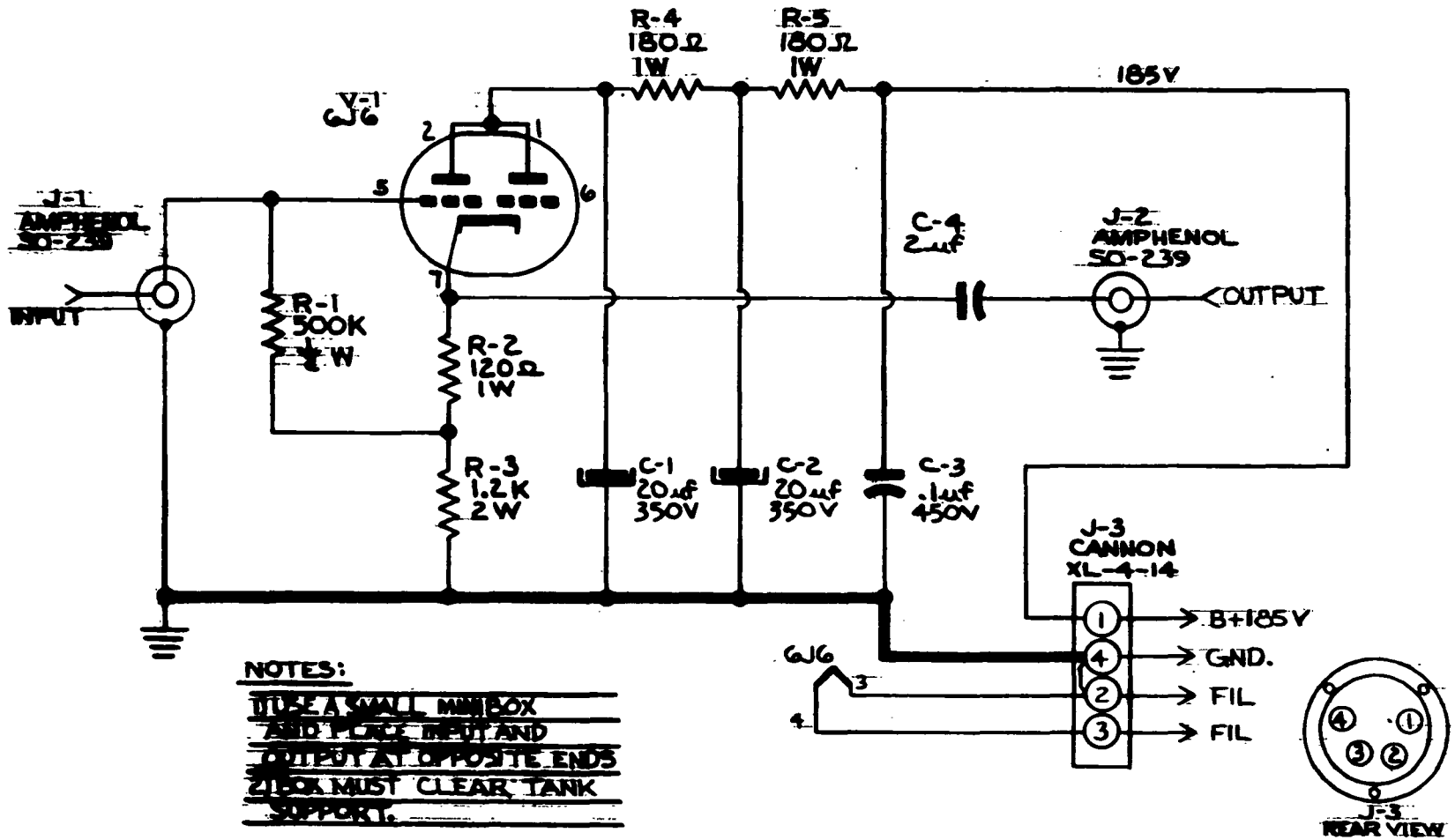

Fig. 3 Cathode follower

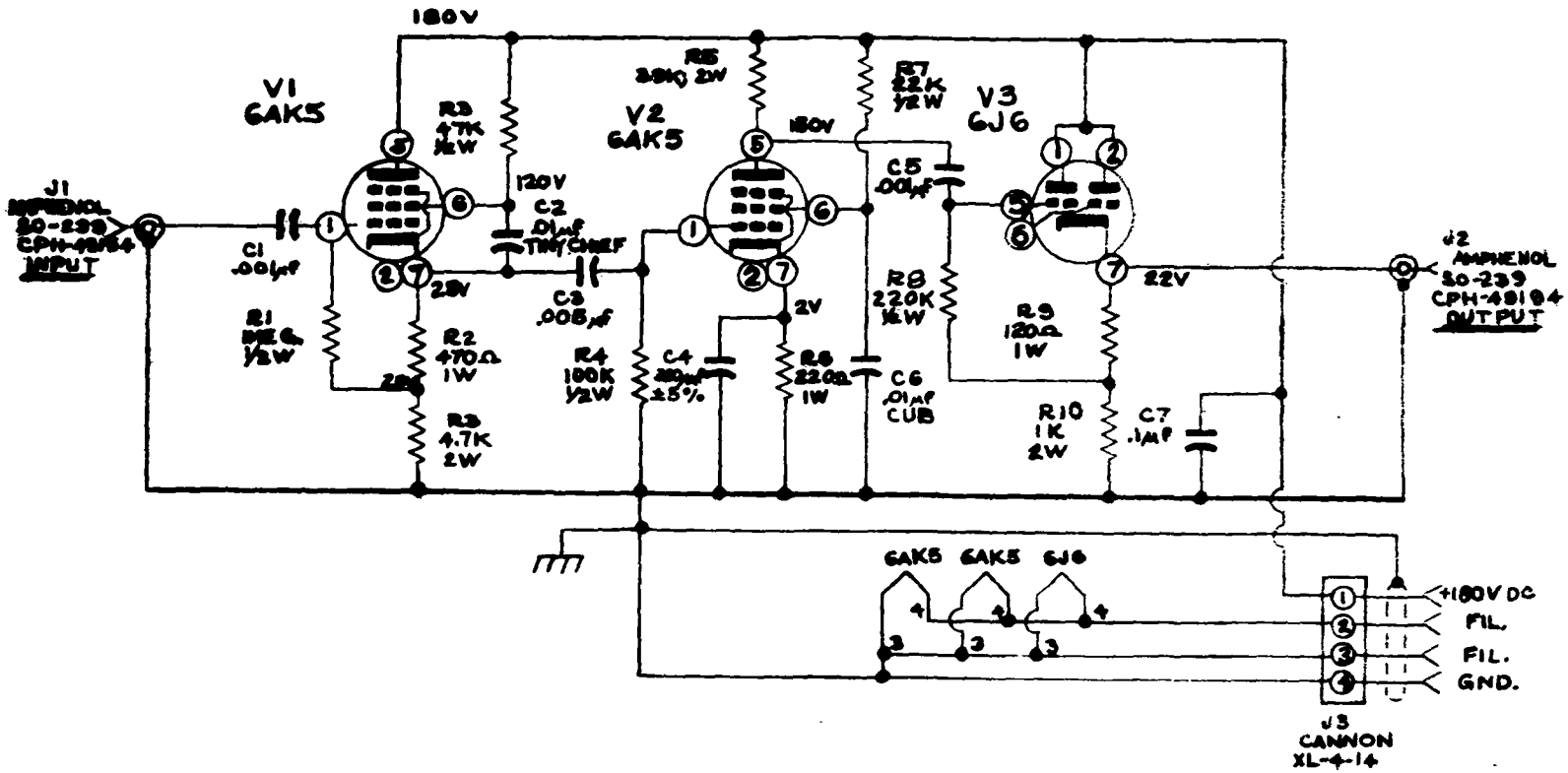

Fig. 4 Video amplifier, 20 db

Developing and Testing Hydrophones

A number of hydrophones using $BaTiO_3$ cylinders but differing in provisions for supporting the crystal were built and tested. Each design produced its own clearly characteristic pulse shape. The conventional form produced extended ringing (Fig. 5a). The hydrophones using Fiberglas insulation as an isolating support for the crystal were also subjected to ringing (Fig. 5b,c). Support b used a limp 6-in. tube of Fiberglas, and Support c used a 1 1/2-in. tube. The design finally adopted was the one having a response most nearly approximating a sharp rise followed by an exponential decay (Fig. 5d). In this model the crystal was mounted on a pair of thin flexible copper wires and supported at the center of a large wire frame by light thread. It is felt that this suspension is superior to those described in the literature.

Five hydrophones of this type were calibrated by USN/USL. The best of these had a sensitivity of -136 db re 1 v/μ bar flat to 150 kc, which fell to -140 db at 500 kc, rose to -131 db at 1000 kc, and fell abruptly to -151 db at 2000 kc. The directivity was negligible up to 200 kc, at which frequency the maximum deviation in sensitivity was $\pm$ 3 db. At 1000 kc, the deviation in sensitivity remained within $\pm$ 3 db for directions perpendicular to the axis of symmetry excepting 10 deg, which was shadowed by the supporting mechanism. These characteristics are shown in Figs. 6 and 7.

Pulse Shapes Obtainable

It has proven impossible with any hydrophone to record perfectly smooth pulse shapes from a spark sound source. This is probably due to no property of the spark other than its short duration.[1,2] (This statement ignores spurious arrivals, a part of whose path lies in the spark electrode. See the next section, "Proper Electrode Geometry.") Several reasons may be advanced for this conclusion:

(1) Oscillations considered to be parasitic on the order of 100 kc or lower can be added or removed by changing the crystal support.

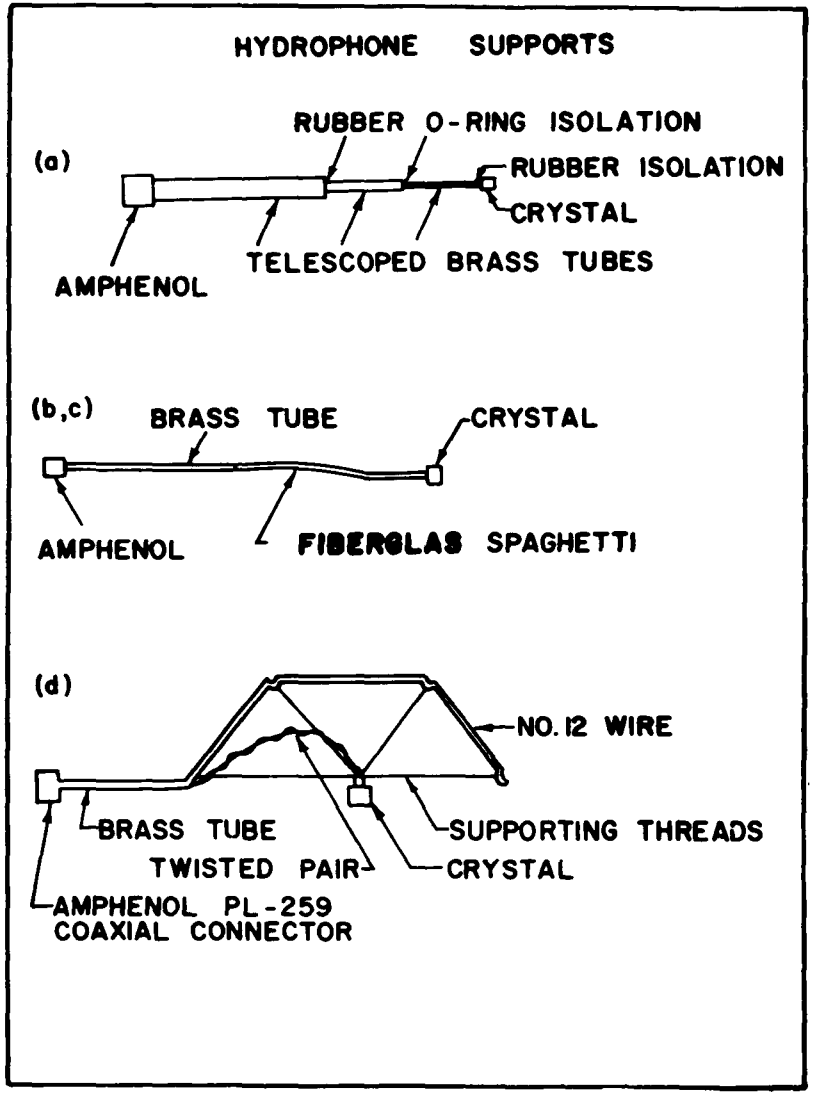

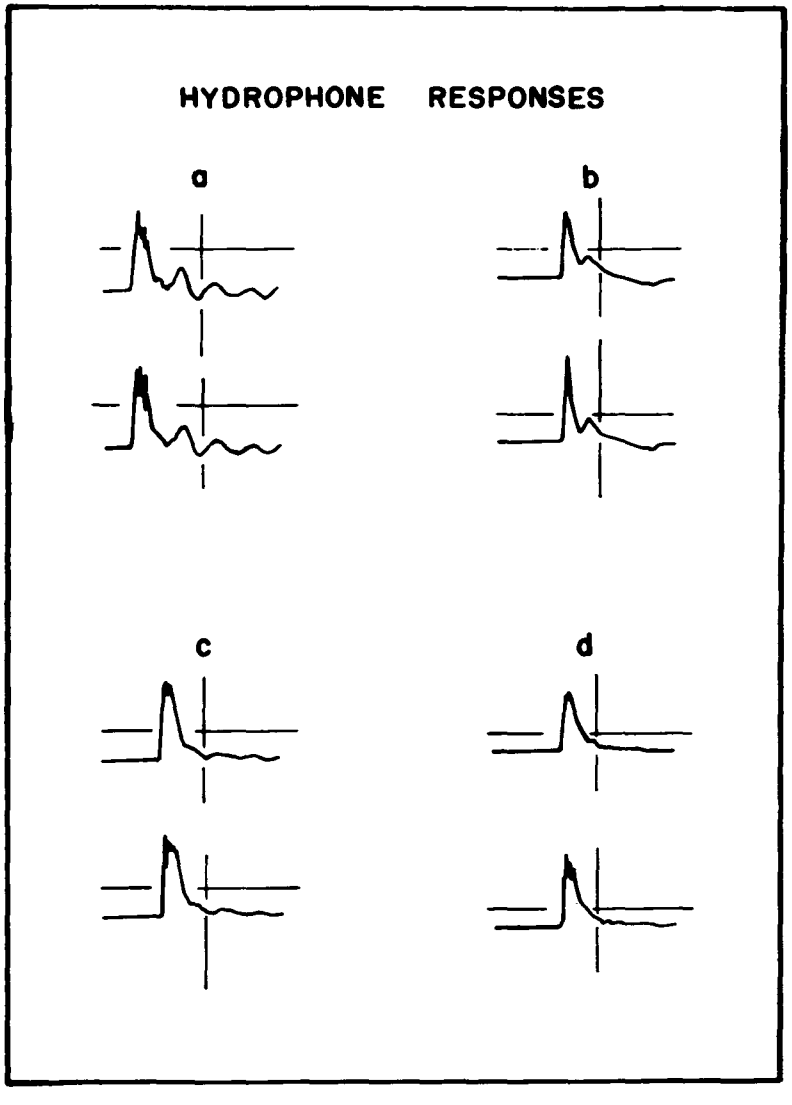

Figure 5

Each type of hydrophone suspension is paired with a typical response (a to a, b to b, etc.). The signal in each case was an underwater spark discharge.

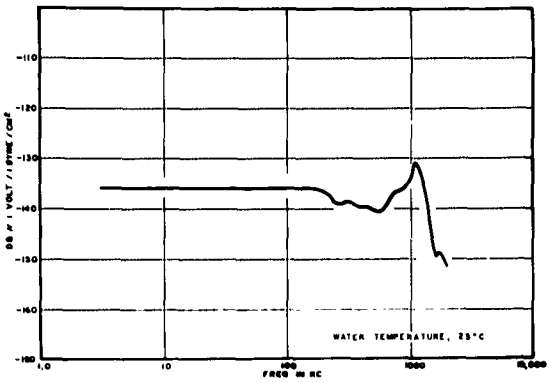

Fig. 6

CHARACTERISTICS OF HUDSON LABORATORIES HIGH-FREQUENCY PROBE NO. 5

Free-field voltage sensitivity (Fig. 6); directivity for 100 kc (Fig. 7a), for 200 kc (Fig. 7b), and for 1000 kc (Fig. 7c)

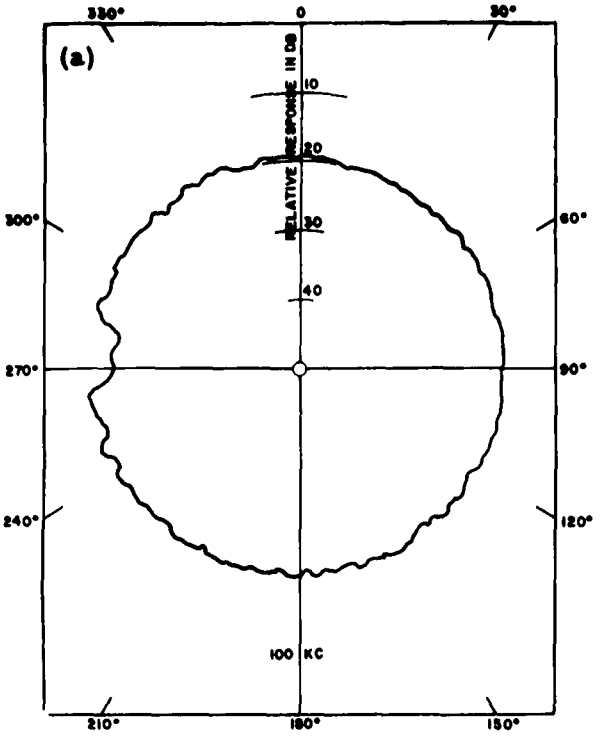

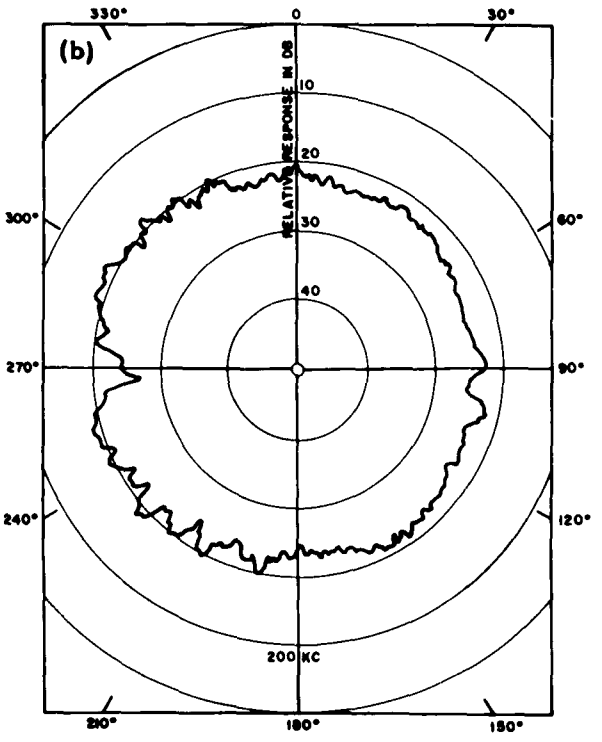

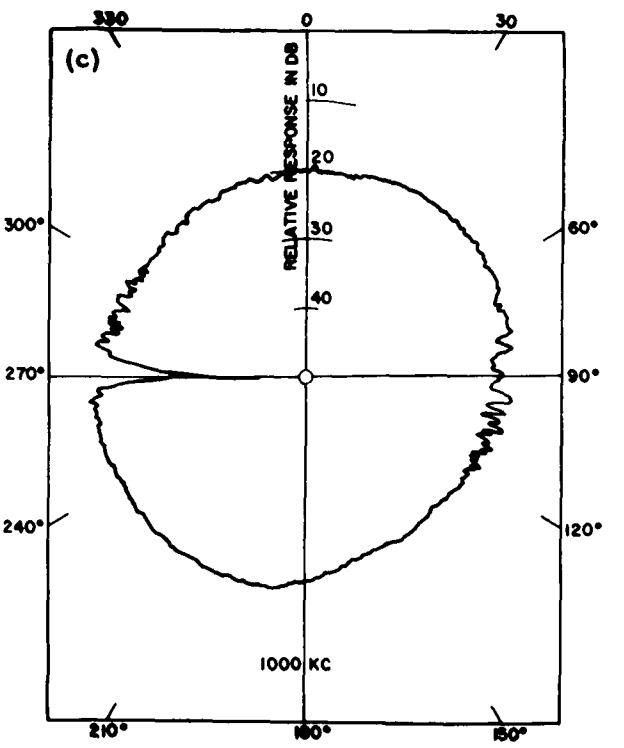

Fig. 7

(2) The bubble left by the spark should have no memory of the exact nature of the spark discharge; however, records of the bubble collapse show the same frequencies of parasitic oscillation as appear in records of the bubble expansion. In fact, since the collapse produces a briefer pressure pulse, these oscillations are much more prominent in records of the collapse (see Fig. 8).

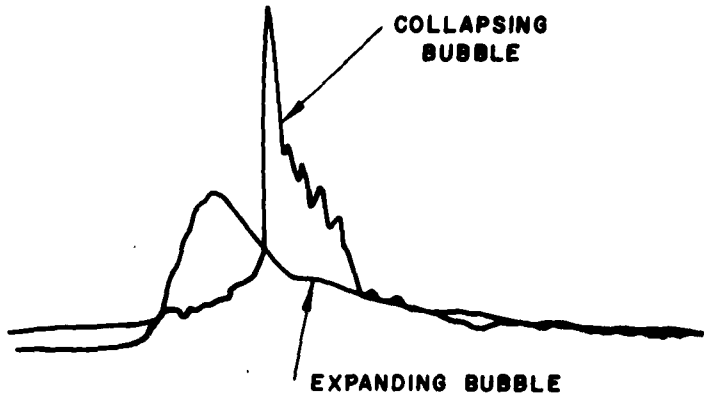

Fig. 8 Pressure pulses produced by a spark discharge and the consequent bubble collapse. The ragged decay is ascribed to resonant oscillation of the receiving crystal.

(3) The parasitic oscillations vary in frequency as the size of the crystal is varied, as shown in Table I.

Table I

Variation of Parasitic Oscillations with Crystal Diameter*

	Apparent Frequencies (kc)		Beat Frequencies (kc)	
Crystal Diameter	a	b	c	d
1/16	910	110	1020	800
1/8	445	106	550	340
1/4	185	400	215	585

* The fluctuations in amplitude typically exhibit two frequencies, a and b. Assuming the observed frequencies are beat frequencies one obtains the component values c and d.

The manufacturer gave the characteristic resonant frequencies of the 1/16-in. crystal as 1060 kc for radial oscillations and 1270 kc for axial oscillations. The loading caused by coating and mounting the crystals lowers their resonant frequencies. Moreover, the resonant frequency of $BaTiO_3$ is a rapid function of temperature. It seems reasonable to assume that mechanical crystal resonances are at least partially responsible for the parasitic oscillations.

(4) These oscillations also vary with changes in the coupling between the crystals and the cable.

Proper Electrode Geometry

Careful examination of records shows that pulses that have traveled some distance along the electrode before leaking into the water may arrive at the hydrophone by several paths. Some may come before and others after the direct water arrival. Measurements show that the velocity of the pressure pulse along the composite brass, plastic, and copper rods that compose the spark electrode is 10,900 ft/sec. Assuming a sound velocity of 4800 ft/sec for water, this yields a critical angle of 26.2 deg.

The geometry of this situation is shown in Fig. 9, where Ω is the critical angle, AS the electrode, S the spark gap, H the hydrophone, and GF the air-water interface. An examination of this geometry shows that the time required for arrival by path SDH is equal to that by the direct path if H lies on the line OS. If H lies within the angle OSA, the pulse taking the path SDH cannot arrive after the direct arrival as long as AS is straight. However, such paths as SCFH and SABH will yield arrivals later than the path SH. These arrivals are large enough to identify.

The use of a curved electrode may displace these arrivals to even more undesirable locations and may even intensify one or more of these arrivals by the focusing action of the curve. It may also add to the number of arrivals by providing new leakage paths. The shape of the electrode must be adjusted in terms of the particular hydrophone locations and time intervals pertinent to a particular investigation. One successful design is shown in Fig. 10.

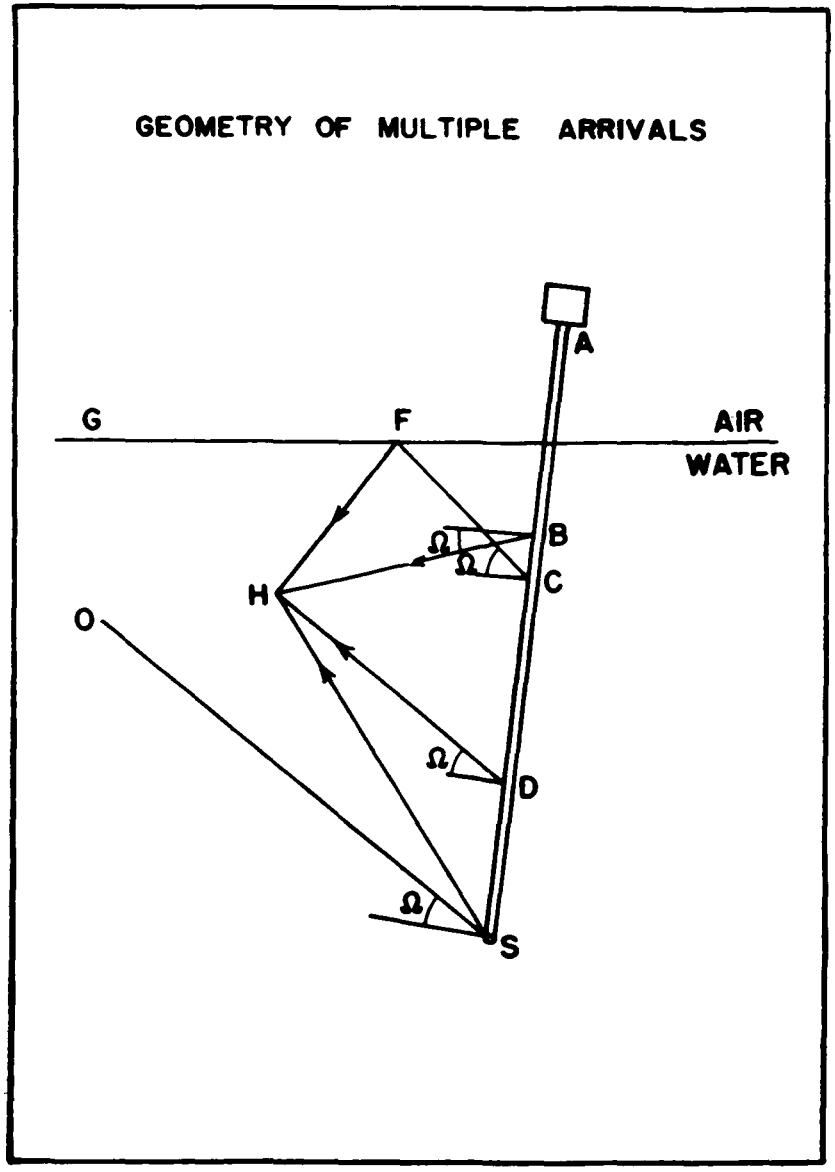

FIGURE 9

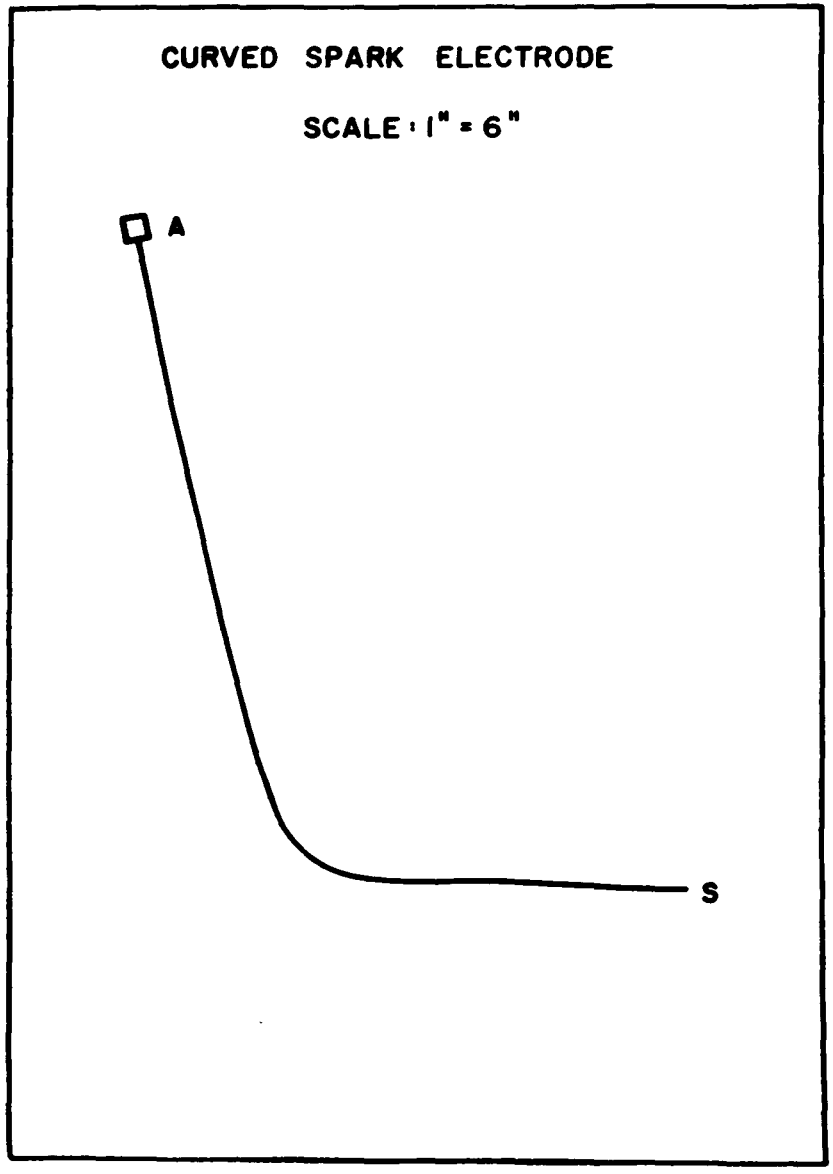

FIGURE 10

BLOCK DIAGRAM FOR CALIBRATION OF VIDEO AMPLIFIER

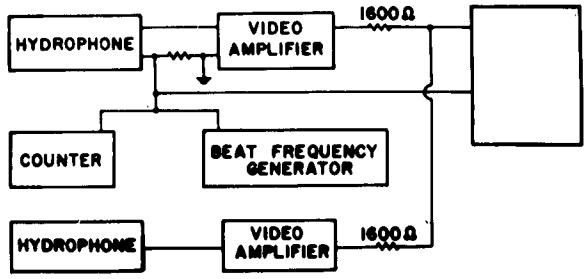

Fig. 11

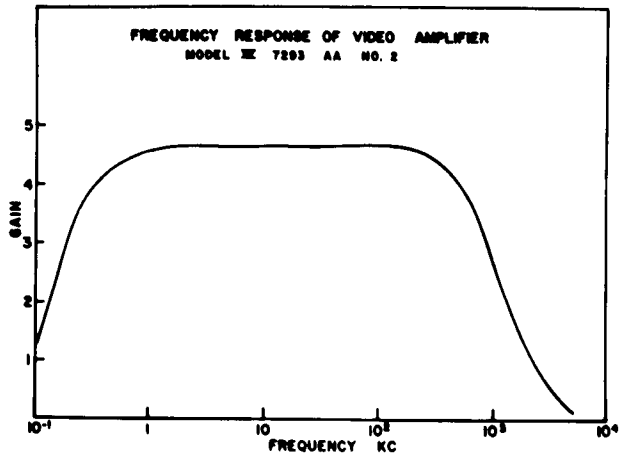

Fig. 12

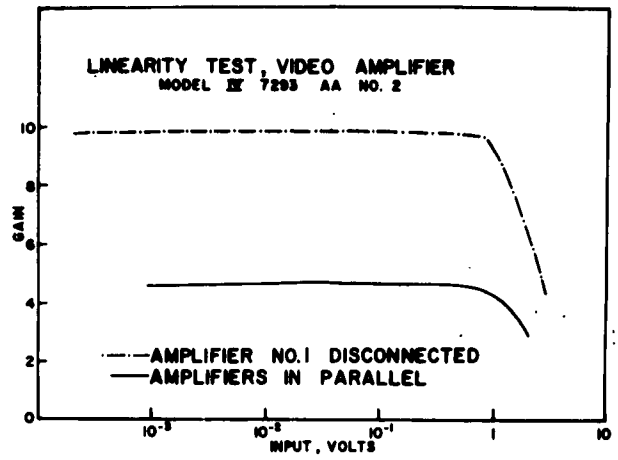

Fig. 13

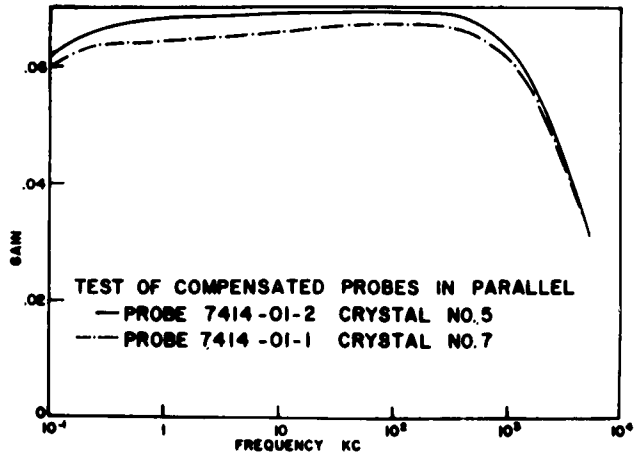

Fig. 14

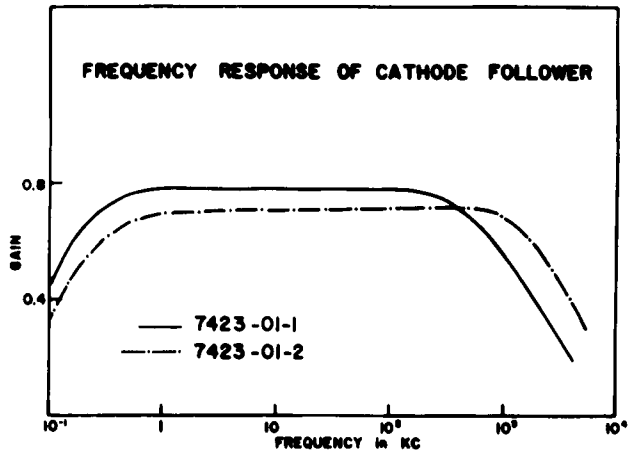

Fig. 15

Matching Hydrophones to Cable

The capacitance of a 1/16-in. $BaTiO_3$ crystal with the mounting leads included is approximately 300 μμf . Its internal resistance is very low, on the order of 1Ω . Comparison of compensated, uncompensated, video-amplifier, and cathode-follower coupling to the scope cable, both by calculation and by experimental tests, indicates that the cathode follower is preferable. The greatest disadvantage of the compensated probes lies in their large attenuation. The disadvantage of the amplifiers lies in their restricted dynamic range. Typical calibration circuits and calibrations appear in Figs. 11-15.

Construction of Spark Gaps

The spark electrodes (see Fig. 16, below) are composed of brass tubing with concentric copper wire insulated from the brass by plastic tubing.* From 100 to 200 sparks can be fired from a 1-μf capacitor charged to 1000 v before the tip of the electrode becomes seriously hollowed. It is quickly restored by a few strokes of a fine file. Ordinarily thousands of sparks can be discharged before the plastic punctures along the length of the electrode.

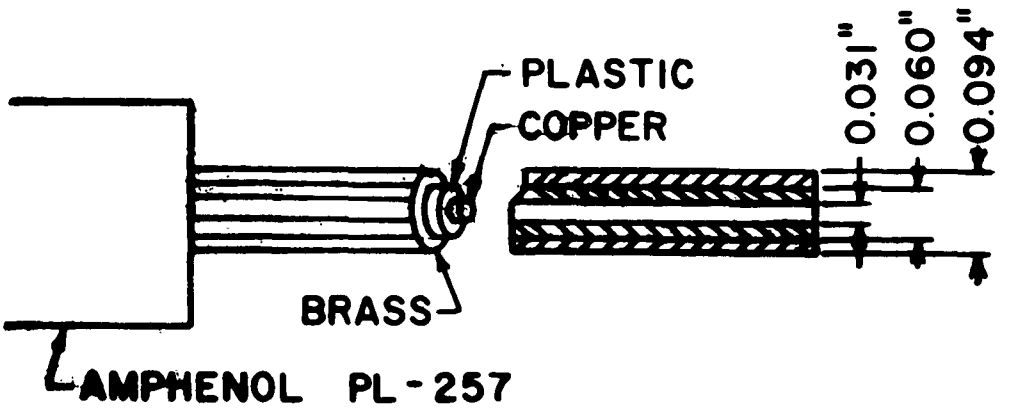

Fig. 16 Spark electrode

* Design suggested by C. S. Clay of the Hudson Laboratories.

These electrodes have been assembled as follows: A piece of brass tubing approximately 18 in. long, outer diameter 0.094 in., and inner diameter 0.060 in. is soldered into an Amphenol PL-257 coaxial connector. Then a length of plastic tubing, Genflex No. 603 Birnbach Biraco tubing size 18, is slowly drawn out until it can be inserted into the brass tubing. Number 20 copper wire is inserted into a part of the plastic which has not yet entered the brass, and then the two together are worked into the brass tube. The plastic tends to draw back to its original length, which makes for a very snug assembly. The copper wire is soldered to the inner coaxial terminal. These assemblies have been operated at up to 2000 v with a useful lifetime.

Directionality of Spark

The directionality of the spark gap was tested by moving a hydrophone in a vertical circle whose center was the spark gap. A comparison hydrophone was kept in a constant location. A comparison of amplitudes is shown in Fig. 17.

It is seen that the length of the electrode represents a preferred direction. The greatest deviation with angle $|A/A_o|_{0\ deg} / |A/A_o|_{150\ deg} = 0.75$ is only slightly greater than the scatter of the data which was averaged for each angle.

There is evidence that the gap may show a larger directivity when pulse shape is considered. This has not been tested with satisfactory controls.

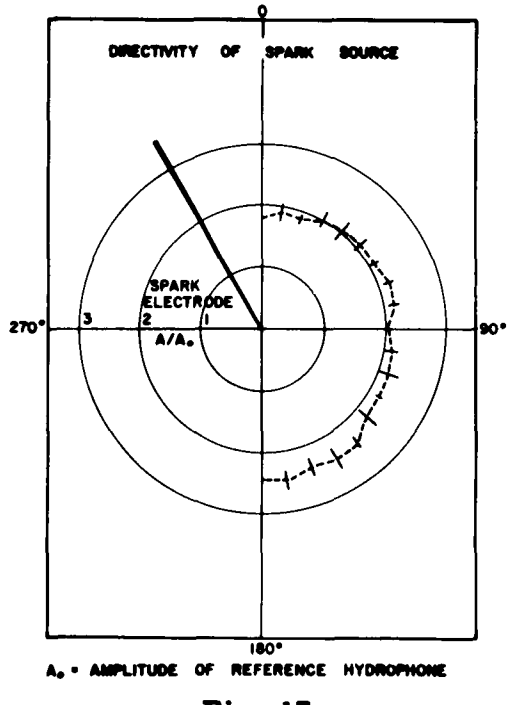

Fig. 17

II. SPARKS AS ANALOGS TO EXPLOSIONS

Scale Models

If experiments performed in a tank are to be planned as models of large-scale phenomena, it is essential that signals be available which will scale with those normally utilized in large-scale studies. In general, as Knopoff points out,[3] the only phenomena that may be scaled are linear.* Cole has shown, however, that the acoustic pulses generated by underwater explosions are nonlinear. Those shock-wave phenomena are usually scaled through the principle of similarity.[4,5]

Underwater sparks also produce shock waves which behave nonlinearly at short ranges. If sparks are to be utilized in model studies it is essential to determine the degree of this nonlinearity and the range beyond which effective linearity may be assumed. In particular it is desirable to know whether the principle of similarity may be extended to spark phenomena, and whether a correspondence may be established between the shock waves produced by explosives and those produced by sparks. This section of the report deals with this problem.

According to A. B. Arons, the peak pressure generated by underwater explosions decreases with range more rapidly than $1/R$, while the time constant increases with range.[5] For TNT and pentolite explosions, he reports the values

$$P_m = 2.16 \times 10^4 \left(\frac{W^{1/3}}{R} \right)^{1.13} \qquad (1)$$

---

* When there is perfect elasticity, $\xi = \alpha \tau$ and $\gamma = 1$ where ξ is the geometric-scale factor, α is the velocity-scale factor, τ is the time-scale factor, and γ is Poisson's ratio-scale factor.
If large-scale experiments in water are to be modeled in water, $\alpha = 1$.

and

$$\frac{\theta}{W^{1/3}} = 58\left(\frac{W^{1/3}}{R}\right)^{-0.22} \tag{2}$$

where P (the peak pressure) is in lb/in.^{2}, W (the weight of explosive detonated) is in lb, R (the range) is in ft, and θ (the time constant) is in microsec. These formulae hold for pressures ranging from 1 lb/in.^{2} to 20,000 lb/in.^{2}.

Combining these two equations to eliminate W yields

$$\frac{\theta}{R} = 5.94 \times 10^{-2} P^{0.69} . \tag{3}$$

Also, by Eq. (1),

$$\frac{P_1}{P_2} = \left(\frac{R_2}{R_1}\right)^{1.13} = \left(\frac{R_1}{R_2}\right)^{-1.13} . \tag{4}$$

The Range-vs-Amplitude Relation

In order to establish the relation between range and amplitude, several sequences of spark discharges have been analyzed with somewhat divergent results; however, in no case is there agreement with the results quoted for explosives.

In these experiments all depths and angular relationships were carefully held constant (see Fig. 18). Hydrophone A_2 was held fixed, and A_1 was moved. The experiment was then repeated as A_1 was held fixed and A_2 was moved. The ratio of the amplitude of the signal at the fixed hydrophone to that at the moving hydrophone was measured and plotted against the ratio of the corresponding range.

The recording techniques used in these experiments are shown in Fig. 19. Each successive experiment is thought to have embodied an improvement in technique. One important improvement in the experiment of May 22, 1958, consisted of a change from a straight spark electrode to a curved one.

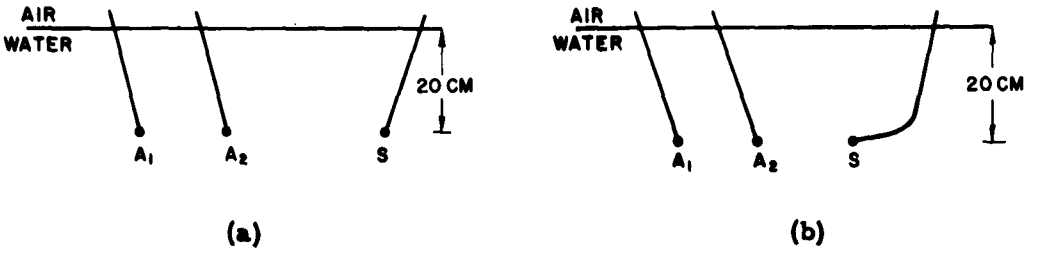

Fig. 18. Configuration (a) was used in the experiments of 30 April 1957, 3 May 1957, and 5 May 1957. Configuration (b) was used in the experiment of 22 May 1958.

A_1 - hydrophone
A_2 - hydrophone
S - spark gap

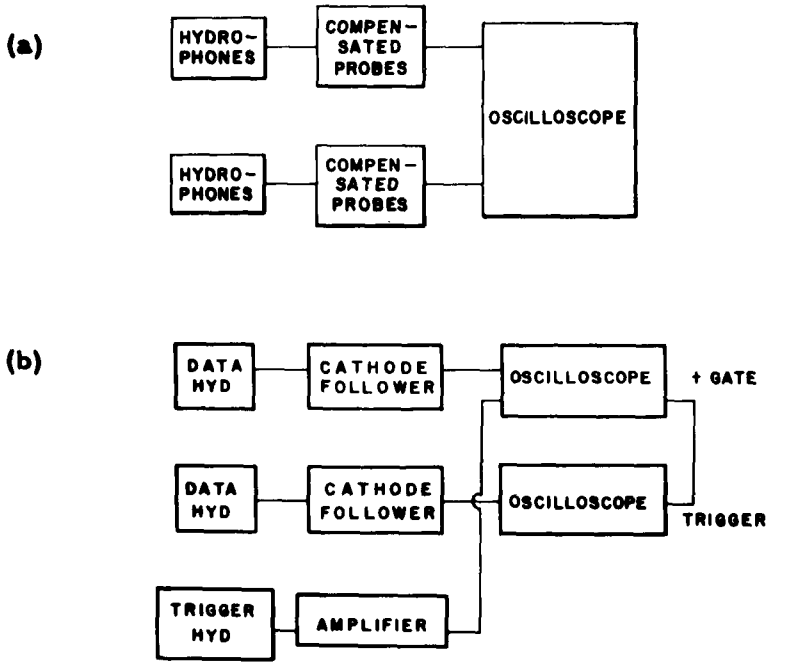

Fig. 19. Equipment in block diagram (a) was used in the experiments of 30 April 1957, 3 May 1957, and 5 May 1957. Equipment in block diagram (b) was used in the experiment of 22 May 1958.

This eliminated the superposition of direct arrivals and arrivals leaking off the electrode. The pulse form was therefore simpler. The correspondence between the particular techniques used and the resulting plot of P_1/P_2 vs R_1/R_2 is indicated by the data appearing in Fig. 20.

When the plots in Fig. 20 are examined to evaluate the exponent in the function

$$\frac{P_1}{P_2} = \left(\frac{R_1}{R_2}\right)^n$$

(see Eq. 4), it is seen that three experiments agree on a value of $n = -0.934$, while the last yields the value $n = -1.01$.

The latter indicates simple geometric spreading; the first three, a falloff slower than geometric. Arons found that $n = -1.13$, i.e., that for explosives the falloff is faster than geometric. It is clear that in regard to pressure vs range, the spark pulses do not show similarity with explosive pulses.

These discrepancies do not arise because the pressures recorded are of a different order of magnitude. Arons' data cover peak pressures ranging from 1 lb/in.^{2} to 20,000 lb/in.^{2}. The experiments being reported recorded pressures ranging from 2 lb/in.^{2} to 60 lb/in.^{2}. Therefore, any differences must be due to either the relative properties of fresh and salt water or the basic pulse shape. Here there is a very real difference. Our time constants may be collected in two groups, one ranging from 2.5 to 5.7 μsec, the other from 9 to 37 μsec. The range of Arons' time constants for the pressure range from 2 lb/in.^{2} to 60 lb/in.^{2}, as calculated from his curves, was from 250 to 380 μsec.

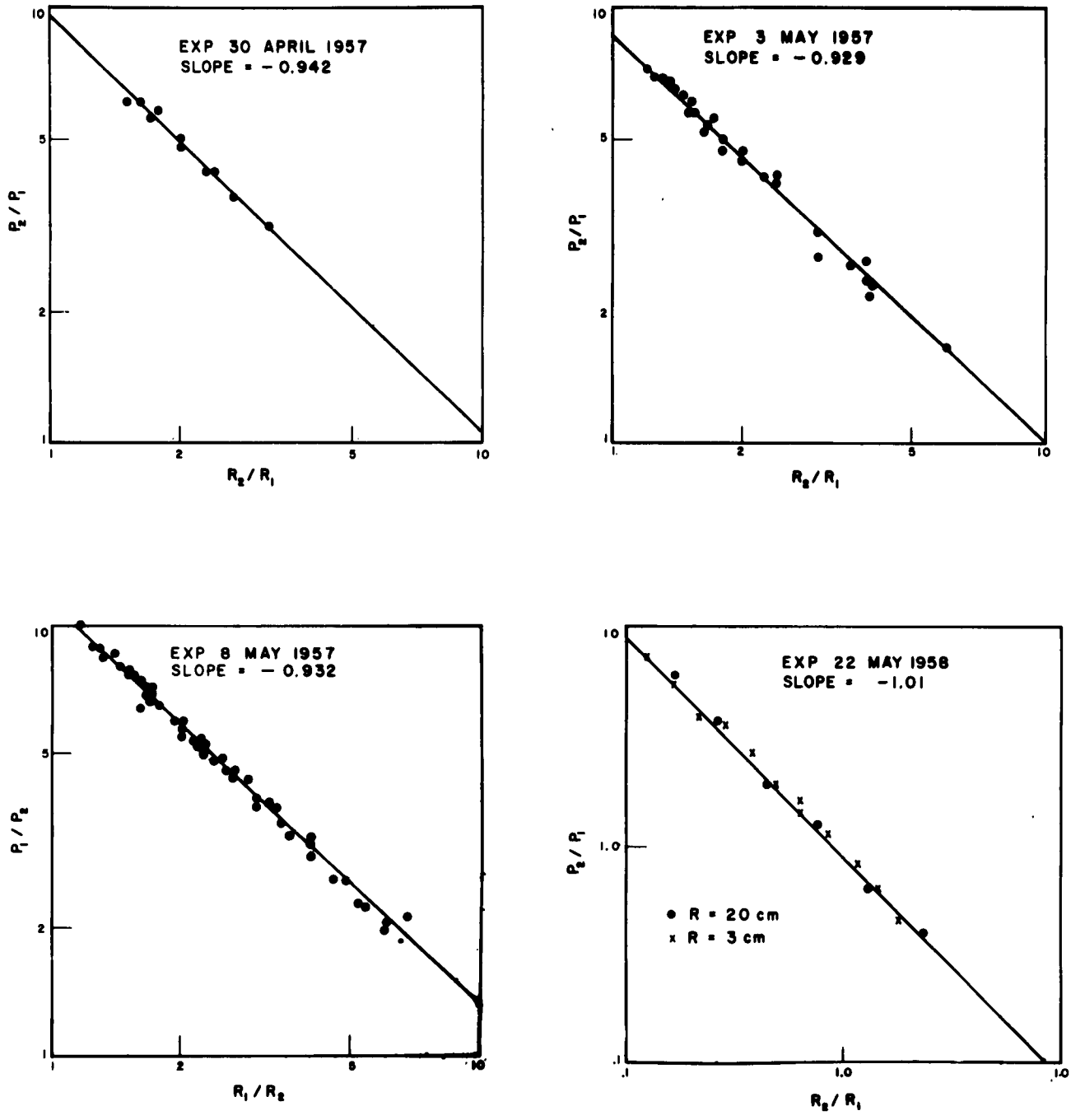

Fig. 20 Plots to evaluate the exponent in $(P_1/P_2) = (R_1/R_2)^n$

The Range-vs-Pulse-Shape Relation

One way of characterizing a pulse shape is in terms of the time constant θ, i.e., the time required for the pressure to decrease in the ratio $P_2/P_1 = 1/e$, where e is the base of the natural logarithm.

Equation (3) of page 16 can be written as

$$\frac{\theta}{\theta_o} \times \frac{R_o}{R} = \left(\frac{P}{P_o}\right)^{0.69} ,$$

the subscript o identifying the particular range, maximum pressure, and time constant corresponding to the reference hydrophone.

A semilog plot of vertical deflection vs time in μsec for one pulse representative of the data taken during the experiment of May 22, 1958, is shown in Fig. 21. The semilog plots were treated in two ways. First, a line was drawn through the rapidly falling spike, and the time constant θ_1 was determined; then, the pulse was treated as the sum of a rapidly varying contribution, θ_2, and a slowly varying contribution, θ_3. These time constants were evaluated for both the reference hydrophone and the movable hydrophone. The results are shown in Fig. 22 (a - f).

Reference to Fig. 22 (a and b) shows that all three time constants are independent of range. This, coupled with the fact that the peak pressure was found to be inversely proportional to range, immediately leads to the first power coefficient found for the function plotted in Fig. 22 (c - f).

The value 1.0 for this coefficient is markedly different from the 0.69 value derived from Arons' explosion data.

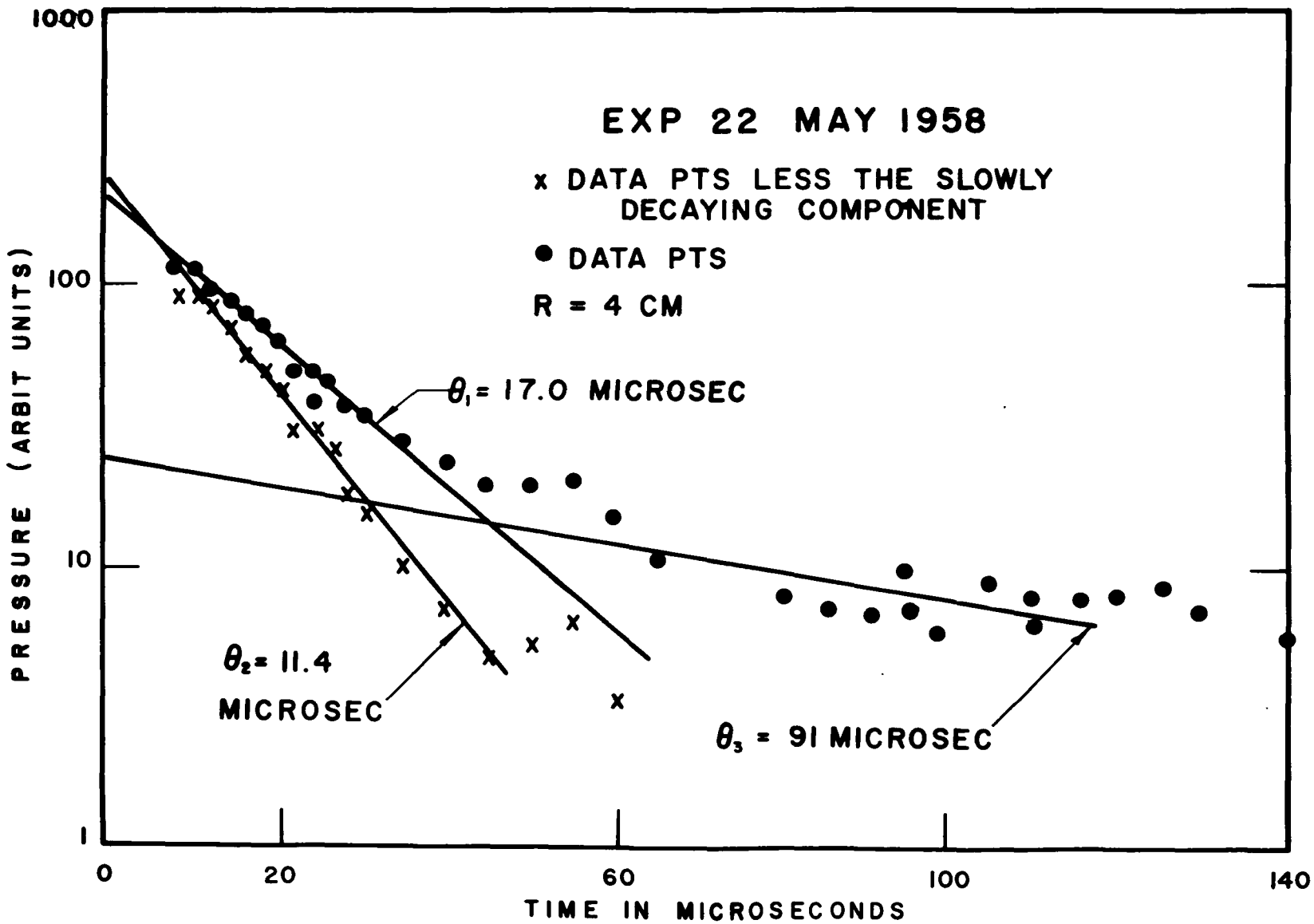

Fig. 21

VERTICAL DEFLECTION VS TIME FOR A TYPICAL PULSE, SHOWING TIME CONSTANTS θ_1, θ_2, AND θ_3

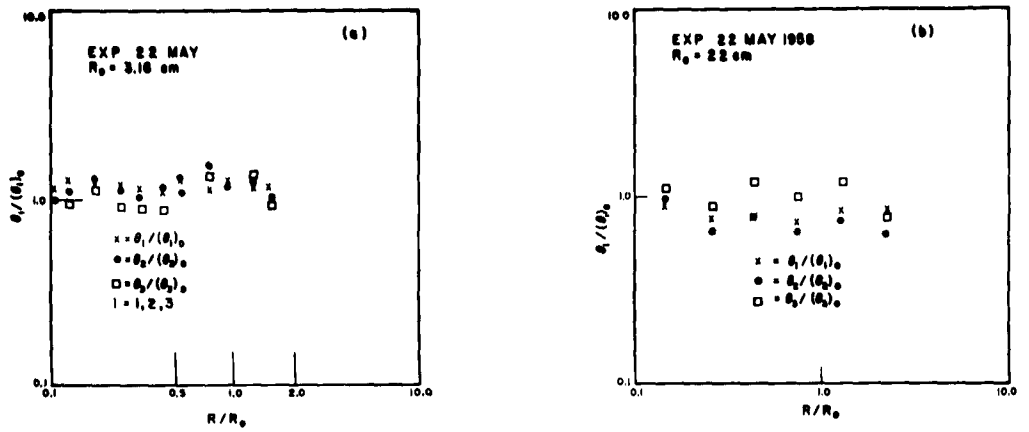

Fig. 22 (a-b)

TIME CONSTANTS θ_1, θ_2, AND θ_3 VS RANGE

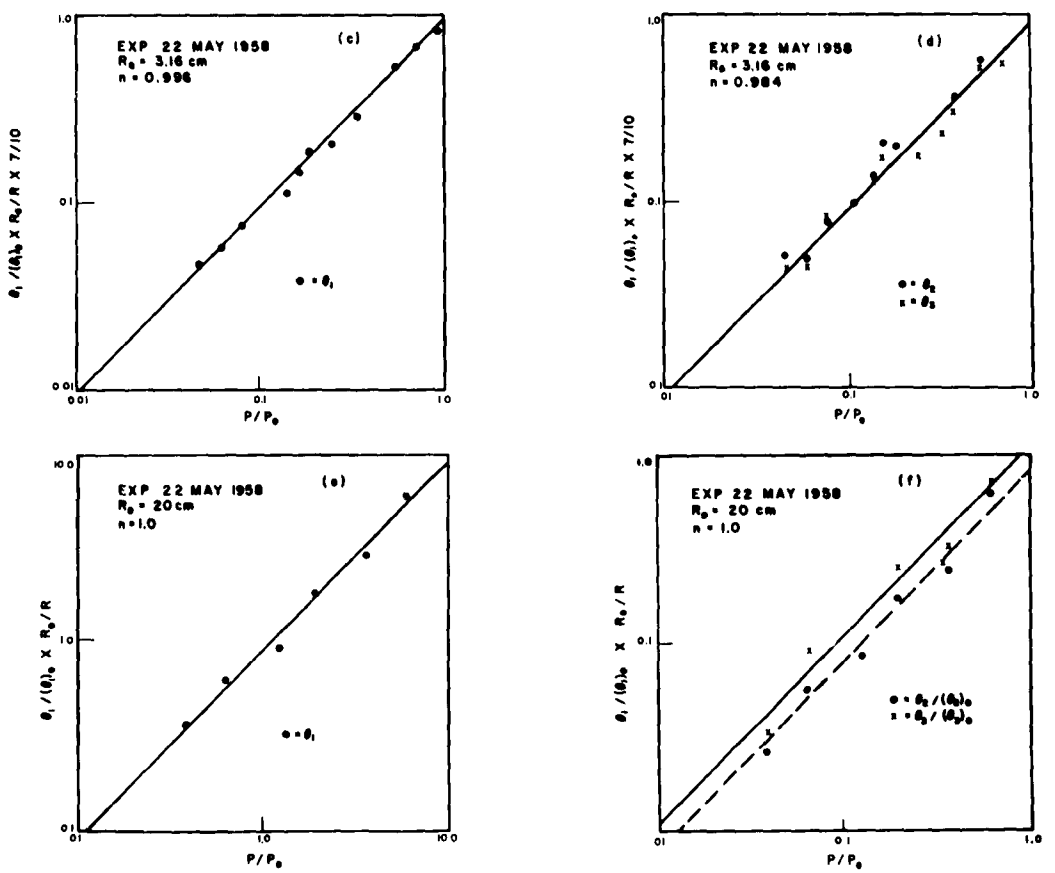

Fig. 22 (c-f)

PLOTS TO EVALUATE THE EXPONENT IN $(\theta/\theta_0)(R_0/R) = (P/P_0)^n$

Resume

The shape of pressure pulses produced by underwater sparks and the decay of these pulses with range have been analyzed. It is concluded that underwater sparks are not suitable as small-scale analogs to explosions in the field. This unsuitability stems from the following:

(1) The peak pressures and time constants of pulses produced by sparks are not related to range in the way of those produced by explosives. The acoustic signals from underwater sparks are transmitted with negligible distortion at ranges which are practical in terms of signal magnitude and geometric limitations. This distortionless transmission makes acoustic signals from underwater sparks unsuitable for comparison with explosive signals.

(2) Successive pulses vary sufficiently so that any evaluation of the relations between variables requires the averaging of many observations for each point graphed.

III. REFLECTION FROM A FREE SURFACE

Reflection of a pressure pulse in water from the air-water interface may be expected to produce a reversal in phase and a possible change in amplitude. These effects may be a function of the frequency as well as the amplitude of the pulse. A corollary to this is that the efficiency of a spark (or any other source) radiating energy in any given direction or the efficiency of a hydrophone as a detector is a function of source or receiver depth (the so-called dipole effect).

Experimental Plan and Instrumentation

On July 24, 1957, experiments were begun to test the dipole effect. In order to simplify the analysis, the angle of reflection (from the air-water interface) was held constant at 30 deg, and the depths of the spark gap and hydrophone were kept equal (see Fig. 23), thus fixing five parameters: the angle of incidence at the air-water interface; the two angles of radiation--from the gap to the surface and from the gap to the hydrophone; and the corresponding two angles of incidence upon the hydrophone. When these parameters are fixed, the depth and separation of the source and receiver can be determined from the travel-time difference between the direct and the reflected pulse.

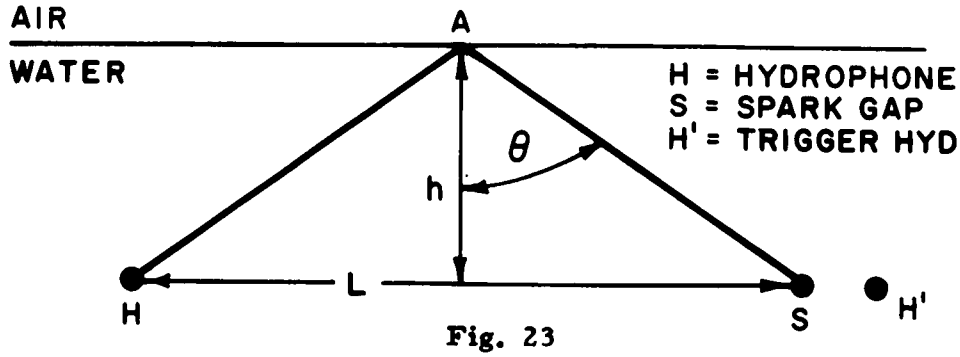

Fig. 23

Geometrical arrangement of hydrophone (H), spark gap (S) and trigger hydrophone (H') in relation to surface.
ΔR = HAS - HS = difference in lengths of direct and reflected paths.

Maintaining a constant potential on the capacitors supplying the spark gap kept the pulses at least statistically similar. If they could have been kept identical the experiment would have been simple; however, fluctuations in amplitude and shape were large. In general, examples differing from the mean by more than about 20 percent were ignored.

ΔR (from the geometry in Fig. 23) was varied from 0.2 to 10 cm. At 0.2 and 0.5 cm the bubble burst the surface.

The block diagram of the electronic system appears in Fig. 24. A second hydrophone acted as trigger for the 531 scope sweep and provided a controllable delay. The positive gate of the 531 activated the 535 trigger and provided a second controllable delay. Thus it was possible to record the direct arrival on the 531 and the reflected arrival on the 535.

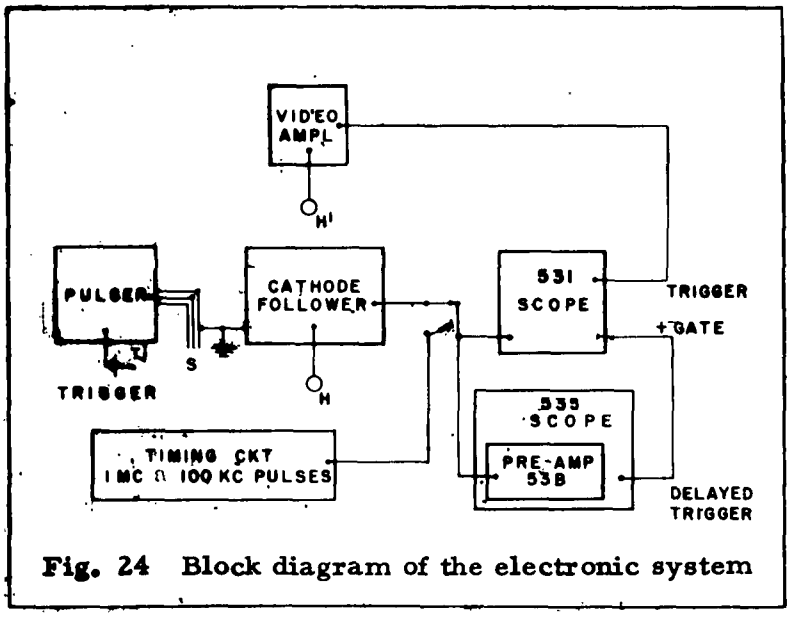

Fig. 24 Block diagram of the electronic system

Considerable overlap was needed to establish a common time base. Enlarged projections of the pulse photographs on 35 mm film were traced on graph paper for convenience of readout.

This data has been analyzed for information about:

(1) The superposition of direct and reflected pulses.

(2) The effect of range on amplitude.

(3) Reflection as a function of angle.

Fourier Analysis of the Data

Pressure was measured as a function of time and tabulated. Fourier analyses were obtained by an IBM 650. Typical analyses are shown in Figs. 25 and 26. The superposition of the direct and reflected pulses produced patterns which were roughly as expected. To a first approximation, reflection produced a 180-deg shift in phase, and the frequency-amplitude spectrum of the composite pulse exhibited the expected maxima and minima.

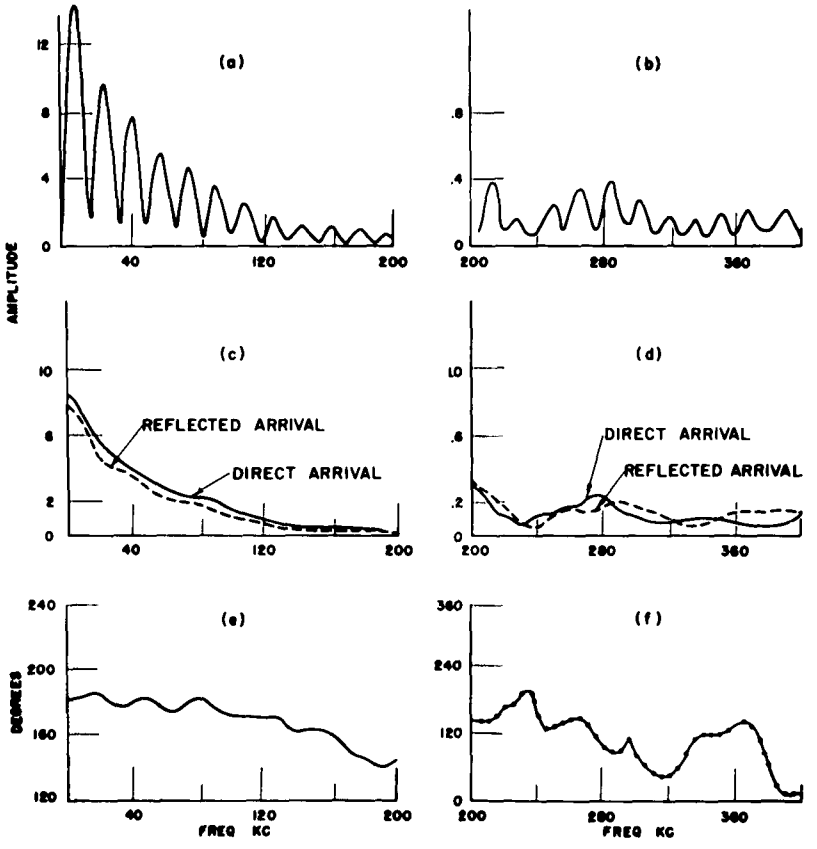

Fig. 25 ΔR = 9 cm
a, b Spectrum of composite pulse
c, d Spectra of separate direct and reflected pulses
e, f Apparent phase shift by reflection

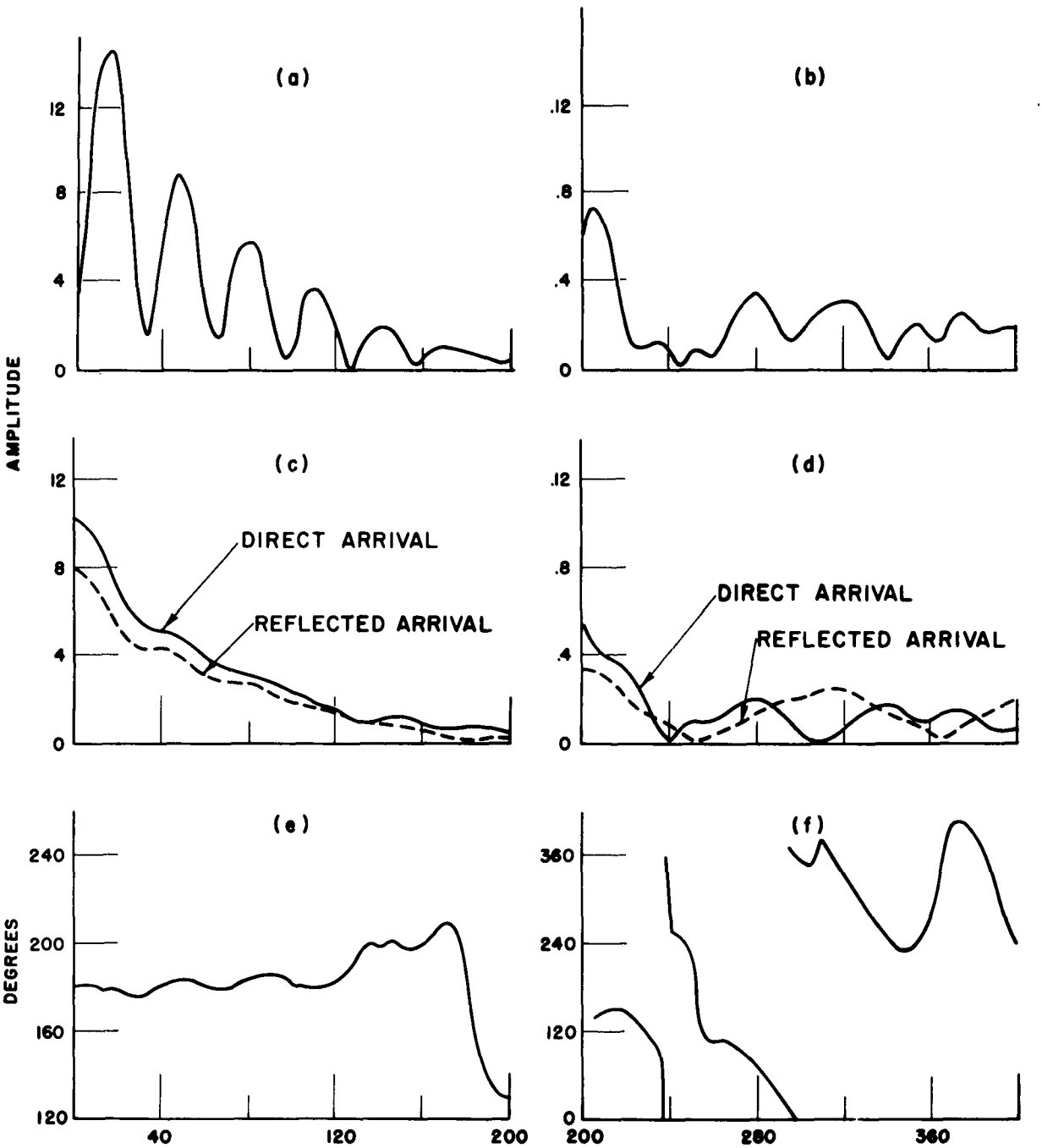

Fig. 26 ΔR = 5 cm
a, b Spectrum of composite pulse
c, d Spectra of separate direct and reflected pulses
e, f Apparent phase shift by reflection

The analysis over the interval T_2 was made by taking differences between an analysis over the interval T_1 and an analysis over the interval $T_1 + T_2$ (Fig. 27), e.g., for a given frequency, the transform of the interval T_1 is $g_1(\omega) = jA_1 \sin \omega t + B_1 \cos \omega t$, and similarly that for $T_1 + T_2$ is $g_{12}(\omega) = jA_{12} \sin \omega t + B_{12} \cos \omega t$; that of the interval T_2, then, is $g_2(\omega) = j(A_{12} - A_1) \sin \omega t + (B_{12} - B_1) \cos \omega t$. $g_1(\omega)$ is considered to be the direct wave, $g_{12}(\omega)$ to be the composite wave, and $g_2(\omega)$ to be the reflected wave (although it obviously contains the tail of the direct wave which, moreover, is unfortunately missing from the analysis in $g_1(\omega)$).

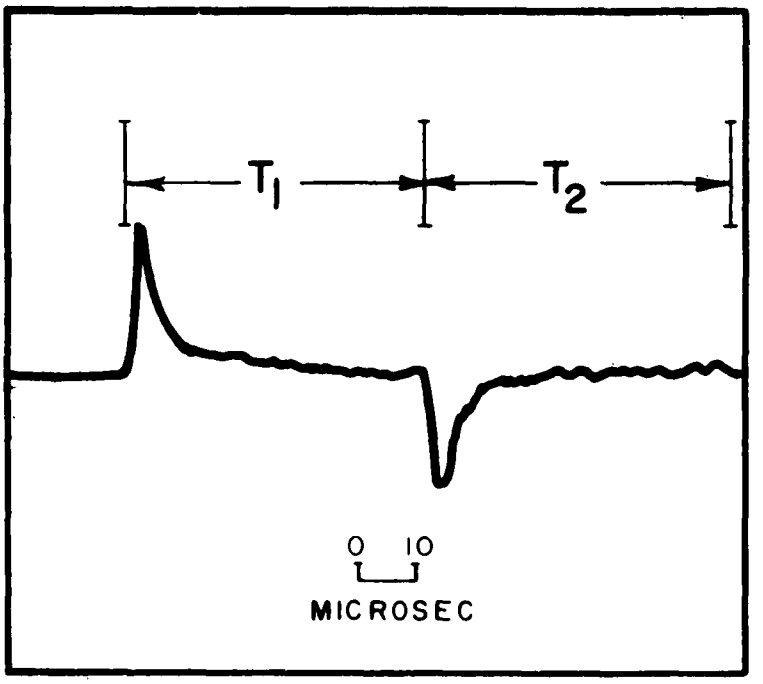

Fig. 27
Typical arrival, direct (T_1) and reflected (T_2)

The phase change due to reflection, δ, was found by the relation $\delta = \theta_R - \theta_D - \phi_\omega$, where $\phi_\omega = 2\pi T_1 \omega$, the phase shift due to range, and where

$$\tan \theta_D = \frac{A_1}{B_1} \qquad \text{and} \qquad \tan \theta_R = \frac{A_{12} - A_1}{B_{12} - B_1} .$$

This produced curves of the type shown in Figs. 25 e, f and 26 e, f.

Results

The curves are extremely well behaved below 200 kc. The erratic behavior at higher frequencies is not surprising for two reasons. One of the cathode followers was not flat above 200 kc; also, the amplitudes of the Fourier components above 200 kc are less than 3 percent of the amplitudes at 10 kc. This would make precision of measurement unlikely. Therefore, little significance should be attached to the curves above 200 kc.

Examination of the results shows that the energy spectrum of the reflected pulse is essentially identical with that of the incident pulse.

However, the phase shift due to reflection shows a smooth periodic fluctuation which is quite unexpected. The characteristics of these fluctuations are summarized in Table II. It is seen that the frequencies at which the maximum phase shift occurs are relatively independent of ΔR .

Table II

Periodicity of Phase Fluctuation Due to Reflection

ΔR cm	Shot No.	Item No.	T_1 μsec	T_2 μsec	f_1* kc	f_2 kc	f_3 kc	f_4 kc
4	2	85-0002	25.25	31.75	16	58	97	136
5	1	0016	32.00	35.00	15	53	87	
	3	0015	32.00	35.00	10+	50	85	134
	5	0012	32.00	34.00	10 ?	50	90	135-145-170?
7	4	0013	50.00	41.00	14	44	70	130-150?
9	1	0014	58.00	42.00	17	45	79	125-150?
	2	0017	59.00	41.00	12	39		

* f_1, f_2, f_3, and f_4 are respectively the first, second, third, and fourth frequencies at which the maximum phase shift occurs.

Effect of Finite Time Intervals and Imperfectly Separated Arrivals on the Analysis

Although the table does not suggest such a relation, it was suspected that the above phenomenon might be due to the fact that the Fourier analyses were made of data which extended over finite rather than infinite time intervals and contained an imperfect separation of direct and reflected arrivals.

In order to get a "feel" for the effect that these two factors might produce, arbitrary pulse shapes were assumed, as follows:

$$f_1(t) = A_D\, e^{-a_D t} + B_D\, e^{-b_D t} \qquad \text{for } 0 < t < T_1 \ ;$$

$$\left.\begin{aligned} f_2(t) = {} & A_D\, e^{-a_D t} + B_D\, e^{-b_D t} \\ & + A_R\, e^{-a_R (t-T_1)} + B_R\, e^{-b_R (t-T_1)} \end{aligned}\right\} \quad \text{for } T_1 < t < T_2 \ .$$

For the meaning of T_1 and T_2, the reader is again referred to Fig. 27.

The Fourier transform of the direct arrival was assumed to be

$$g_D(\omega) = \int_0^{T_1} f_1(t)\, e^{j\omega t}\, dt \ .$$

The transform of the reflected arrival was assumed to be

$$g_R(\omega) = \int_{T_1}^{T_1 + T_2} f_2(t)\, e^{j\omega (t-T_1)}\, dt \ .$$

These shapes are simpler than the experimental pulses, but they do contain provisions for both a slow and a fast decay rate, as well as three suspect assumptions implicit in the IBM analysis:

(1) That cutting off the direct wave at $t = T_1$ yields a sufficiently accurate determination of $g_D(\omega)$.

(2) That cutting off the reflected wave at $t = T_1 + T_2$ yields a sufficiently accurate determination of $g_R(\omega)$.

(3) That the direct wave need not be subtracted out of the "reflected wave" in order to obtain the true reflected wave.

As T_1 and T_2 increase, the above assumptions become more and more tenable.

When $\tan\theta_D$ and $\tan\theta_R$ are constructed from these Fourier transforms one obtains

$$\tan\theta_D = \frac{\frac{A_D}{a_D^2+\omega^2}[\omega(1-\alpha_c)-a_D\alpha_s]+\frac{B_D}{b_D^2+\omega^2}[\omega(1-\beta_c)-b_D\beta_s]}{\frac{A_D}{a_D^2+\omega^2}[a_D(1-\alpha_c)+\omega\alpha_s]+\frac{B_D}{b_D^2+\omega^2}[a_D(1-\beta_c)+\omega\beta_s]}$$

$$\tan\theta_R = \frac{\frac{A_D e^{-a_D T_1}}{a_D^2+\omega^2}[\omega(1-\gamma_c)-a_D\gamma_s]-\frac{A_R}{a_R^2+\omega^2}[\omega(1-\gamma_0)-a_R\gamma_s]+B_D e^{-b_D T_1}[\omega(1-\zeta_c)-b_D\zeta_s]-\frac{B_R}{b_R^2+\omega^2}[\omega(1-\zeta_c)-b_R\zeta_s]}{\frac{A_D e^{-a_D T_1}}{a_D^2+\omega^2}[a_D(1-\gamma_c)+\omega\gamma_s]-\frac{A_R}{a_R^2+\omega^2}[a_D(1-\gamma_c)+\omega\gamma_s]+\frac{B_D e^{-b_D T_1}}{b_D^2+\omega^2}[b_D(1-\zeta_c)+\omega\zeta_s]-\frac{B_R}{b_R^2+\omega^2}[b_R(1-\zeta_c)+\omega\zeta_s]}$$

where

$\alpha_c = e^{-a_D T_1}\cos\omega T_1$ $\qquad$ $\gamma_c = e^{-a_R T_2}\cos\omega T_2$

$\alpha_s = e^{-a_D T_1}\sin\omega T_1$ $\qquad$ $\gamma_s = e^{-a_R T_2}\sin\omega T_2$

$\beta_c = e^{-b_D T_1}\cos\omega T_1$ $\qquad$ $\zeta_c = e^{-b_R T_2}\cos\omega T_2$

$\beta_s = e^{-b_D T_1}\sin\omega T_1$ $\qquad$ $\zeta_s = e^{-b_R T_2}\sin\omega T_2$

As $\omega \to 0$, $\tan\theta_D \to \frac{+\omega}{+a_D}$ and therefore $\theta_D \longrightarrow 0$ deg. Also, when $\omega \to 0$, $\tan\theta_R \longrightarrow 0$, and since all the exponential terms (e.g., $e^{-a_D T_1}$) are small compared to 1, the numerator and denominator of $\tan\theta_R$ are negative. Therefore, $\theta_R = 180$ deg. Thus one predicts the observed 180-deg phase shift at $\omega = 0$. Shot 85-0016, for which R = 5 cm, supplies a typical set of constants:

Table III

Decay Constants of Direct and Reflected Pulses

Direct	Reflected
$T_1 = 31.5\ \mu\text{sec}$	$T_2 = 44.75\ \mu\text{sec}$
$a_D = 4.3 \times 10^5\ \text{sec}^{-1}$	$a_R = 3.7 \times 10^5\ \text{sec}^{-1}$
$b_D = 0.81 \times 10^5\ \text{sec}^{-1}$	$b_R = 0.32 \times 10^5\ \text{sec}^{-1}$
$e^{-a_D T_1} = 1/(8 \times 10^5)$	$e^{-a_R T_2} = 1/(15 \times 10^6)$
$e^{-b_D T_1} = .078$	$e^{-b_R T_2} = 0.24$
$A_D = 710$ to 430	$A_R = 91$
$B_D = 47$ to 36	$B_R = 17.8$

It is seen from Table III that the effect of clipping off the tails of the pulses is very small, that is, exponential terms involving the short time constant are negligible by the time that $t = T_1$ (in the case of the direct arrival) or $t = T_1 + T_2$ (in the case of the reflected arrival), while the terms involving the long time constant are small. If these terms could be neglected completely, one could write

$$\tan\theta_D = \frac{+\omega}{+a_D} \quad ; \quad \tan\theta_R = \frac{-\omega\left(\frac{A_R}{a_R^2+\omega^2} + \frac{B_R}{b_R^2+\omega^2}\right)}{-a_R\left(\frac{A_R}{a_R^2+\omega^2} + \frac{B_R}{b_R^2+\omega^2} \times \frac{b_R}{a_R}\right)} \quad .$$

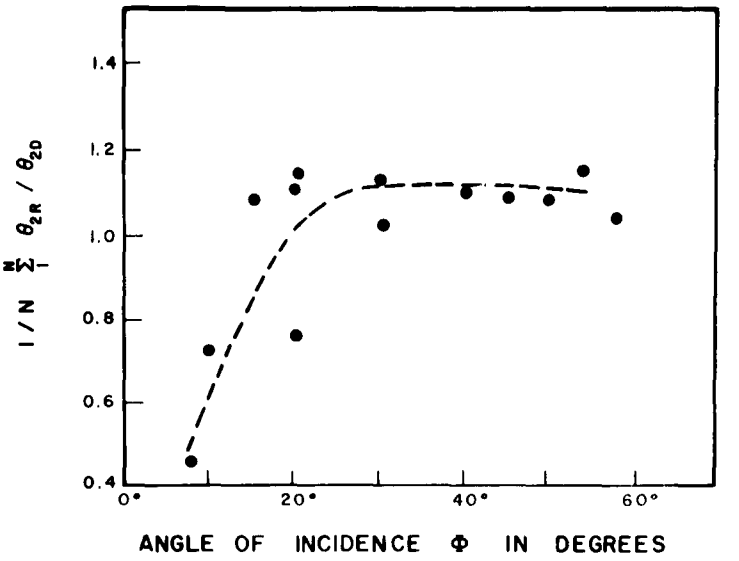

Fig. 28 Modification of time constant by reflection: short time constant

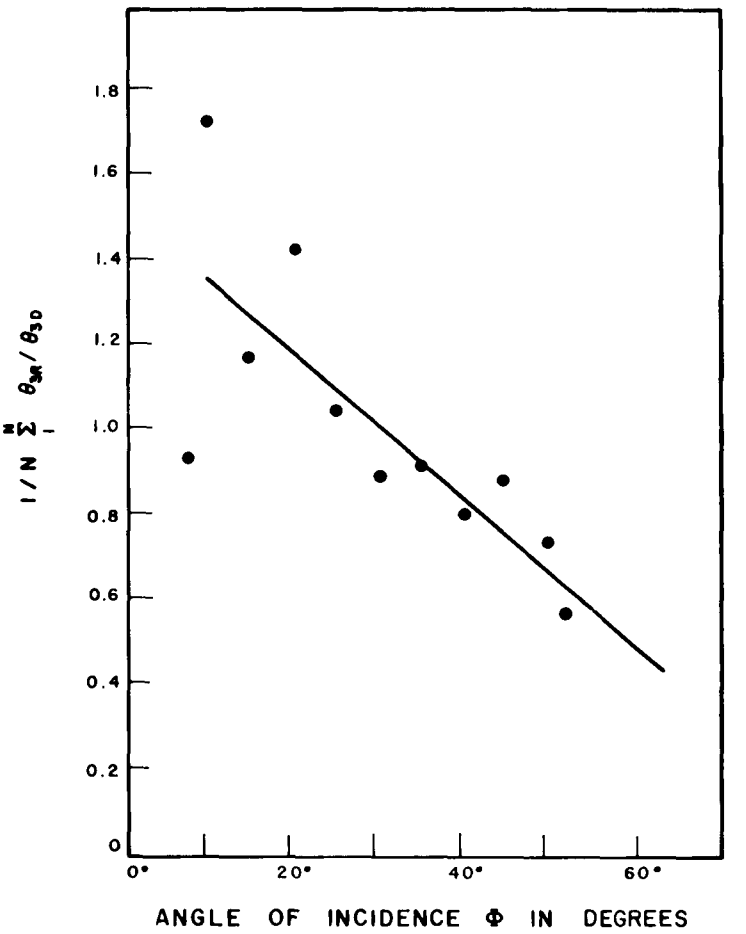

Fig. 29 Modification of time constant by reflection: long time constant

These expressions produce a phase shift upon reflection that becomes progressively less than 180 deg as frequency increases, but that has no oscillations. The expressions containing the effects of clipping would surely oscillate. Although the oscillations of Table II do not show a recognizable relation to the clipping constants T_1 and T_2, the above discussion does throw doubt on the validity of the observation that the phase shift due to reflection from an air-water interface is a function of frequency. Independent verification is needed.

Reflection as a Function of Angle

It was felt that if the phase shift caused by reflection was a function of frequency, it would probably be a function of the angle of incidence also, and if so, that the time constant of the reflected pulse would also be a function of angle of incidence. The possibilities of this line of attack were therefore investigated.

Several sets of data were taken. These were all in rough agreement. What appears to be the best set is shown in Figs. 28 and 29. The symbols θ_1, θ_2, and θ_3 have the meaning assigned in Part II, "The Range-vs-Pulse-Shape Relation." (See page 20.) The geometry is shown in Fig. 30.

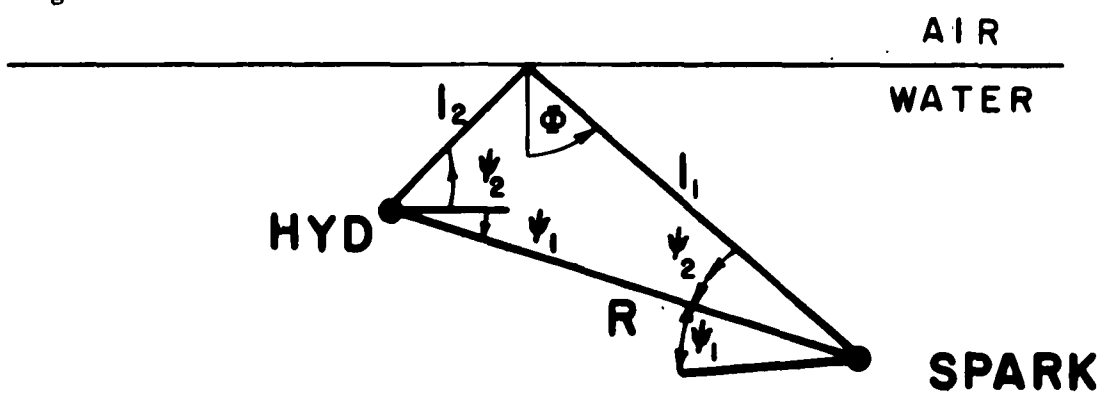

Fig. 30
Geometry of spark and hydrophone relative to surface

The recording system was that of Fig. 1, except that only one scope was used; therefore, both direct and reflected pulses were recorded on a single frame of film. For the set of data reported here, $l_1 = 20$ cm , and $l_1 + l_2 - R = 8$ cm . With these parameters held constant, Ψ_1 and Ψ_2 are a function of Φ. This unfortunately injects the problem of the directionality of the spark gap and hydrophone. Reference to the calibrations appearing in Part I of this report shows that the directionality of the hydrophone is certainly small at all frequencies below 200 kc. The directionality of the spark gap is somewhat larger but not over 2 db .

Bubbles rising from the spark gap tend to modify the region directly above the spark gap. This affects the data corresponding to normal incidence. When this effect was discovered it was minimized by firing the sparks at longer intervals.

It is felt that the results shown in Figs. 28 and 29 are at least qualitatively correct and that the short time constant is shortened by reflection at small angles of incidence, while the long time constant is longest at normal incidence and shortest at larger angles of incidence.

REFERENCES

1. Robert H. Mellen, "An experimental study of the collapse of a spherical cavity in water," J. Acoust. Soc. Am. 28, 447-454 (1956).
2. Halden L. Smith and Harold C. Early, Experimental Studies of Underwater Sparks. University of Michigan, Engineering Research Institute Project 2048, July 1953.
3. L. Knopoff, "Small three-dimensional seismic models," Trans. Am. Geophys. Union 36, 1029 (1955).
4. Robert H. Cole, Underwater Explosions (Princeton University Press, Princeton, N. J., 1948).
5. A. B. Arons, "Underwater explosion shock wave parameters at large distances from the charge," J. Acoust. Soc. Am. 26, 343-346 (1954).

HUDSON LABORATORIES

DISTRIBUTION LIST

Office of Naval Research
Department of the Navy
Washington 25, D. C.
(Code 466) copies 1-2
(Code 468) copy 3

Commanding Officer and Director
U. S. Navy Underwater Sound Laboratory
Fort Trumbull
New London, Connecticut
copies 4-5

Director
U. S. Naval Ordnance Laboratory
White Oak
Silver Spring 19, Maryland
copies 6-7

Commander
U. S. Naval Ordnance Test Station
China Lake, California
Attn: Technical Director
copy 8

Commander (Code 753)
U. S. Naval Ordnance Test Station
China Lake, California
Attn: Technical Library
copy 9

Commander
U. S. Naval Ordnance Test Station
Pasadena Annex
3202 East Foothill Boulevard
Pasadena 8, California
Attn: Pasadena Annex Library
copy 10

Director
Marine Physical Laboratory
University of California
Scripps Institution of Oceanography
San Diego 52, California
copy 11

Director
Bell Telephone Laboratories
Whippany, New Jersey
copies 12-13

Committee on Undersea Warfare
National Research Council
National Academy of Sciences
2101 Constitution Avenue
Washington 25, D. C.
copies 14-15

Chief
Bureau of Ships
Department of the Navy
Washington 25, D. C.
(Code 688) copies 16-17
(Code 341) copy 18

The Hydrographer
U. S. Navy Hydrographic Office
Washington 25, D. C.
copies 19-20

Director
Naval Research Laboratory
Washington 20, D. C.
Attn: Code 5500, Dr. H. L. Saxton
copies 21-22

Commanding Officer and Director
U. S. Navy Electronics Laboratory
Point Loma
San Diego 52, California
copies 23-24

Commander
U. S. Naval Air Development Center
Johnsville, Pennsylvania
copies 25-26

Dr. F. V. Hunt
Harvard University
Cambridge, Massachusetts
copy 27

Director
Woods Hole Oceanographic Institution
Woods Hole, Massachusetts
copy 28

Director
Columbia University
Lamont Geological Observatory
Torrey Cliff
Palisades, New York
copy 29

Officer in Charge
MWDP Contract Supervisory Staff
SACLANT ASW Research Center
APO 19, New York, New York
via (1)
Office of Naval Research (Code 466)
via (2)
Chief of Naval Operations (Op-92C2)
Washington 25, D. C.
via (3)
Secretariat
State-Defense Military Information
Control Committee
Pentagon
Washington 25, D. C.
copy 30

Chief
Bureau of Naval Weapons (RUDC-252)
Department of the Navy
Washington 25, D. C.
copies 31-32

Chief
Bureau of Weapons
Department of the Navy
Washington 25, D. C.
(Code RU) copies 33-34
(Code RU-222) copy 35

Chief of Naval Operations
Department of the Navy
Washington 25, D. C.
(Op-001) copy 36
(Op-03EG) copy 37
(Op-07T) copy 38
(Op-312) copies 39-40
(Op-716) copies 41-43

Commanding Officer
ONR Branch Office
Navy No. 100
Fleet Post Office
New York, New York
copies 44-45

Commander
Armed Services Technical
Information Agency
Arlington Hall Station
Arlington, Virginia
copies 46-55, 79-88

Commander
Submarine Development Group II
U. S. Naval Submarine Base
Box 70
New London, Connecticut
copies 56-57

Weapons Systems Evaluation Group
Office of Sec'y of Defense
Room 1E875 Pentagon Building
Washington 25, D. C.
copy 58

Commanding Officer
ONR Branch Office
346 Broadway
New York 13, New York
copy 59

Special Representative
Hudson Laboratories
Dobbs Ferry, New York
Attn: Mr. Shandler
copy 60

Commanding Officer and Director
David Taylor Model Basin
Washington 7, D. C.
copies 61-62

Commanding Officer and Director
U. S. Naval Underwater Ordnance
Station
Newport, Rhode Island
copy 63

Director
Applied Physics Laboratory
University of Washington
Seattle, Washington
copy 64

Director
Ordnance Research Laboratory
Pennsylvania State University
University Park, Pennsylvania
via
Production Representative
Ordnance Research Laboratory
University Park, Pennsylvania
copy 65

Superintendent
U. S. Naval Post Graduate School
Monterey, California
copies 66-67

Institute for Defense Analysis
Communications Research Division
von Neumann Hall
Princeton, New Jersey
copy 68

The Director
Systems Analysis Group
Undersea Warfare Research and Development Planning Council
U. S. Naval Ordnance Laboratory
White Oak
Silver Spring, Maryland
copy 69

Director
National Oceanographic Data Center
Bldg. 160, U. S. Naval Weapons Plant
Washington 25, D. C.
copy 70

July 1962

UNCLASSIFIED CATALOG CARDS

Hudson Labs., Columbia Univ., Dobbs Ferry, N. Y. THE SPARK GAP AS AN ACOUSTIC SOURCE, by M. Vertner Brown and James Ricard. October 30, 1959. 42 p. (Technical rept. no. 80; CU-101-62-ONR-266-Phys.) (Contract Nonr-266(84)) Unclassified report

This report describes and evaluates a model system for studying the transmission of acoustic signals through the water. Spark sources were studied with special reference to whether the acoustic signals generated by sparks scale with those generated by explosions. It is shown that they do not.

The surface reflection of these pulses was also studied. A phase shift as a function of frequency and a change in pulse shape as a function of angle of incidence were observed.

An extended series of experiments was performed, each experiment incorporating new parameter controls and/or improved apparatus and techniques, the most (over)

1. Sparks-Acoustic properties
2. Underwater sound reflection-Analysis
3. Underwater sound transmission-Model studies

I. Brown, M. Vertner
II. Ricard, James
III. Contract Nonr-266(84)

Hudson Labs., Columbia Univ., Dobbs Ferry, N. Y. THE SPARK GAP AS AN ACOUSTIC SOURCE, by M. Vertner Brown and James Ricard. October 30, 1959. 42 p. (Technical rept. no. 80; CU-101-62-ONR-266-Phys.) (Contract Nonr-266(84)) Unclassified report

This report describes and evaluates a model system for studying the transmission of acoustic signals through the water. Spark sources were studied with special reference to whether the acoustic signals generated by sparks scale with those generated by explosions. It is shown that they do not.

The surface reflection of these pulses was also studied. A phase shift as a function of frequency and a change in pulse shape as a function of angle of incidence were observed.

An extended series of experiments was performed, each experiment incorporating new parameter controls and/or improved apparatus and techniques, the most (over)

1. Sparks-Acoustic properties
2. Underwater sound reflection-Analysis
3. Underwater sound transmission-Model studies

I. Brown, M. Vertner
II. Ricard, James
III. Contract Nonr-266(84)

Hudson Labs., Columbia Univ., Dobbs Ferry, N. Y. THE SPARK GAP AS AN ACOUSTIC SOURCE, by M. Vertner Brown and James Ricard. October 30, 1959. 42 p. (Technical rept. no. 80; CU-101-62-ONR-266-Phys.) (Contract Nonr-266(84)) Unclassified report

This report describes and evaluates a model system for studying the transmission of acoustic signals through the water. Spark sources were studied with special reference to whether the acoustic signals generated by sparks scale with those generated by explosions. It is shown that they do not.

The surface reflection of these pulses was also studied. A phase shift as a function of frequency and a change in pulse shape as a function of angle of incidence were observed.

An extended series of experiments was performed, each experiment incorporating new parameter controls and/or improved apparatus and techniques, the most (over)

1. Sparks-Acoustic properties
2. Underwater sound reflection-Analysis
3. Underwater sound transmission-Model studies

I. Brown, M. Vertner
II. Ricard, James
III. Contract Nonr-266(84)

Hudson Labs., Columbia Univ., Dobbs Ferry, N. Y. THE SPARK GAP AS AN ACOUSTIC SOURCE, by M. Vertner Brown and James Ricard. October 30, 1959. 42 p. (Technical rept. no. 80; CU-101-62-ONR-266-Phys.) (Contract Nonr-266(84)) Unclassified report

This report describes and evaluates a model system for studying the transmission of acoustic signals through the water. Spark sources were studied with special reference to whether the acoustic signals generated by sparks scale with those generated by explosions. It is shown that they do not.

The surface reflection of these pulses was also studied. A phase shift as a function of frequency and a change in pulse shape as a function of angle of incidence were observed.

An extended series of experiments was performed, each experiment incorporating new parameter controls and/or improved apparatus and techniques, the most (over)

1. Sparks-Acoustic properties
2. Underwater sound reflection-Analysis
3. Underwater sound transmission-Model studies

I. Brown, M. Vertner
II. Ricard, James
III. Contract Nonr-266(84)

successful of which are reported here. Particular attention was directed to the problem of reducing stray arrivals through proper support of the hydrophones and the spark gap.

successful of which are reported here. Particular attention was directed to the problem of reducing stray arrivals through proper support of the hydrophones and the spark gap.

successful of which are reported here. Particular attention was directed to the problem of reducing stray arrivals through proper support of the hydrophones and the spark gap.

successful of which are reported here. Particular attention was directed to the problem of reducing stray arrivals through proper support of the hydrophones and the spark gap.